

**Climate impact on mean annual cycle and interannual variability of CO<sub>2</sub> fluxes in European DBF and ENF forests: insights from observations and state-of-the-art data-driven and process-based models**

Asmat Ullah<sup>1</sup>, Julien Crétat<sup>1</sup>, Gaïa Michel<sup>1,2</sup>, Olivier Mathieu<sup>1</sup>, Mathieu Thevenot<sup>1</sup>, Andrey Dara<sup>3</sup>, Robert Granat<sup>3</sup>, Zhendong Wu<sup>4,5</sup>, Clément Bonnefoy-Claudet<sup>1</sup>, Julianne Capelle<sup>1</sup>, Jean Cacot<sup>6</sup>, John S. Kimball<sup>7</sup>

<sup>1</sup> Biogéosciences, UMR 6282 CNRS, Université Bourgogne Europe, Dijon, France

<sup>2</sup> AgroParisTech, 91120, Palaiseau, France

<sup>3</sup> CarbonSpace Ltd., D04H1F3 Dublin, Ireland

<sup>4</sup> Department of Physical Geography and Ecosystem Science, Lund University, Lund, Sweden

<sup>5</sup> ICOS ERIC, Carbon Portal, Lund, Sweden

<sup>6</sup> Bibracte, Glux-en-Glenne, France

<sup>7</sup> Numerical Terradynamic Simulation Group, University of Montana, Missoula, MT, United States of America

Correspondence to: Julien Crétat ([julien.cretat@ube.fr](mailto:julien.cretat@ube.fr))

58 **Abstract.**

59

60 The impact of climate on the annual cycle and interannual variability of CO<sub>2</sub> fluxes is assessed in European  
61 evergreen needleleaf (ENF) and deciduous broadleaf (DBF) forests using observations from 19 sites, alongside  
62 outputs from process-based and data-driven models. All models capture the temporal phasing of CO<sub>2</sub> fluxes,  
63 including a shorter sequestration period in northern than southern Europe, a more pronounced annual cycle for  
64 DBFs than ENFs in central Europe, and strong interannual variability across sites. However, they generally  
65 underestimate both the magnitude of CO<sub>2</sub> sequestration and its interannual variability compared to observations.  
66 Along the annual cycle, all datasets indicate enhanced CO<sub>2</sub> uptake from late spring to early fall, with a stronger  
67 climate-CO<sub>2</sub> flux coupling in northern and central Europe than in southern Europe, where seasonality is less  
68 pronounced. At the interannual timescale, the climate does not show a significant influence on observed and  
69 modelled NEE, when correlations are computed using monthly anomalies across all months combined. This  
70 apparent lack of relationship conceals meaningful seasonal patterns. In winter and fall, NEE tends to be positively  
71 correlated with temperature, soil moisture and VPD. In spring, NEE shows negative correlations with temperature  
72 and VPD, but a positive correlation with soil moisture. The summer pattern is reversed compared to the spring  
73 pattern. In the observations, these relationships are noisy in both time and space, suggesting strong site-specific  
74 effects. In contrast, the models exhibit more structured and spatially coherent patterns with strong correlations,  
75 which may reflect an exaggerated response to climate forcing despite underestimated magnitude in CO<sub>2</sub> flux  
76 interannual variability.

77

78 **Key words:** Net ecosystem exchange, gross primary production, ecosystem respiration, climate, annual cycle,  
79 interannual variability, DBF, ENF

80

**a supprimé:** output

**a supprimé:** We first evaluate the models' ability to reproduce observed patterns before using them as complementary tools to investigate climate influences.

**a supprimé:** the

**a supprimé:** CO<sub>2</sub>

**a supprimé:** the

**a supprimé:** all

**a supprimé:** struggle to accurately reproduce the magnitude of observed fluxes,

**a supprimé:** underestimating

**a supprimé:** strength

**a supprimé:** compared to observations

**a mis en forme :** Indice

**a mis en forme :** Non Exposant/ Indice

**a supprimé:** cross all datasets

**a supprimé:** sequestration

**a supprimé:** is favored under relatively hot and dry conditions

**a supprimé:** from late spring to early fall

**a supprimé:** . The coupling between climate and CO<sub>2</sub> fluxes is, however,

**a supprimé:** climate

**a mis en forme :** Indice

**a supprimé:**

**a supprimé:** impact on observed CO<sub>2</sub> fluxes

**a supprimé:** appears spatially noisy due to limited temporal coverage and differences in data availability across sites. Despite uncertainties, the models provide a clearer picture of climate influences, revealing spatial and seasonal variations. Atmospheric factors (i.e., 2 m temperature and vapor pressure deficit) primarily drive interannual CO<sub>2</sub> flux variability in northern and central Europe, whereas soil moisture plays a dominant role in southern Europe

**a mis en forme :** Anglais (E.U.)

**a mis en forme :** Anglais (E.U.)

**a mis en forme :** Anglais (E.U.)

**a mis en forme :** Anglais (E.U.)

**a mis en forme :** Indice

**a supprimé:** Winter and fall CO<sub>2</sub> release increases with elevated temperature and VPD in northern and central Europe but under low VPD in southern Europe. In northern and central Europe, CO<sub>2</sub> sequestration is enhanced by anomalously hot and dry conditions in spring, while by anomalously cold and wet conditions in summer. In southern Europe, CO<sub>2</sub> sequestration is also favored by anomalously cold and wet conditions from May to September

**a mis en forme :** Anglais (E.U.)

## 1 Introduction

Forest ecosystems are the largest part of the land CO<sub>2</sub> sink (Lindeskog et al., 2021), with up to 20-50% of anthropogenic CO<sub>2</sub> emissions (land-use changes excluded) sequestered for the 2000-2010 period (Le Quéré et al., 2018; Pugh et al., 2019; Pan et al., 2024). In Europe, recent estimations suggest a slight increase in CO<sub>2</sub> sequestration by forest ecosystems over the 2000-2021 period mainly due to the fertilization effect of increased atmospheric CO<sub>2</sub> concentration (Prentice et al., 2001; Piao et al., 2009; Schimel et al., 2015; Walker et al., 2020; Sitch et al., 2024). This trend remains, however, weak, because the fertilization effect has almost been compensated by a decrease in CO<sub>2</sub> sequestration induced by climate change (Sitch et al., 2024). The extent to which climate controls CO<sub>2</sub> flux exchanges between the atmosphere and European forest ecosystems is thus a burning question in the context of climate change.

Numerous studies have demonstrated the strong influence of climate on CO<sub>2</sub> exchanges between the atmosphere and forest ecosystems. The annual cycle, and to a lesser extent, interannual variability of these fluxes, are driven by factors such as incident shortwave radiation, temperature, atmospheric evaporative demand, and the water cycle, including soil moisture dynamics (Haszpra et al., 2005; Tang et al., 2014; von Buttlar et al., 2018; Kong et al., 2022; Sharma et al., 2022; Li et al., 2023; Xu et al., 2023). The dominant climate factor influencing CO<sub>2</sub> fluxes depends on the specific component considered. The variability in net ecosystem exchanges (NEE) is a mixed response of its two components: gross primary production (GPP), which sequesters CO<sub>2</sub> into the ecosystem through photosynthesis, and ecosystem respiration (RECO), which releases CO<sub>2</sub> into the atmosphere from forest metabolism (autotroph respiration) and the decomposition of organic matter by fungi and bacteria (heterotrophic respiration). GPP is primarily driven by vapour pressure deficit (VPD), shortwave radiation, temperature, and soil moisture, while RECO is mainly influenced by precipitation, soil moisture, and temperature (Messori et al., 2019).

The influence of climate on CO<sub>2</sub> fluxes also depends on several additional factors, with seasonality playing a crucial role. Severe heat waves and droughts acted to reduce CO<sub>2</sub> sequestration in summer at the Europe-wide scale in 2003 (Ciais et al., 2005), in northern Europe in 2018 (Smith et al., 2020; Thompson et al., 2020) and in central and southeastern Europe in 2022 (van der Woude et al., 2023). On the other hand, anomalously high temperature under normal soil moisture conditions in spring set favourable growth conditions, hence increased CO<sub>2</sub> sequestration, such as in northern Europe in 2018 (Smith et al., 2020). The climatic zone under consideration is also a key factor. For instance, GPP is mostly influenced by soil moisture in the Mediterranean region, VPD over parts of central Europe and temperature over Scandinavia, parts of eastern and south-eastern Europe and higher elevations (Seddon et al., 2016; Madani et al., 2017). The influence of climate on CO<sub>2</sub> flux exchanges is further shaped by various factors, including soil properties (Kurbatova et al., 2008; Besnard et al., 2018; Curtis and Gough, 2018; Martinez del Castillo et al., 2022), forest management practices (Carrara et al., 2003; Saunders et al., 2012), tree age (Kurbatova et al., 2008; Besnard et al., 2018) and tree species (Carrara et al., 2003; Carrara et al., 2004; Welp et al., 2007; Kong et al., 2022).

Assessing the impact of climate on CO<sub>2</sub> flux exchanges remains challenging. The main reason involves the scarcity of multi-year CO<sub>2</sub> fluxes measured by eddy covariance above the canopy (Burba, 2021). At the European scale,

the Integrated Carbon Observation System (ICOS) network provides standardized and open data from 98 ecosystem stations across 16 countries. The flux tower measurements remain limited in number and temporal depth and unevenly distributed spatially, making it difficult to assess the impact of climate on the interannual variability (and trends) in CO<sub>2</sub> flux exchanges and to map them. Process-based and data-driven models allow us to tackle the above limitations. Process-based models, such as dynamical vegetation models, are routinely used to assess CO<sub>2</sub> flux exchanges between the atmosphere and the biosphere (Friedlingstein et al., 2023). These are mechanistic models (Friedlingstein et al., 2006; Sitch et al., 2008) allowing for testing the response of CO<sub>2</sub> fluxes to individual and combined forcing (Sitch et al., 2024). Data-driven models rely on the identification of statistical relationships between flux tower measures by eddy-covariance and corresponding land use, vegetation properties and climate characteristics. Based on these statistical relationships, empirical models are built and used for upscaling, i.e., for assessing CO<sub>2</sub> fluxes in regions where they are not measured (Tramontana et al., 2016; Jung et al., 2019; Jung et al., 2020; Zhuravlev et al., 2022). Both approaches have limitations. Estimations of CO<sub>2</sub> flux exchanges are highly sensitive to physical parameterizations (Cai and Prentice, 2020) and atmospheric forcing (Wu et al., 2017; Hardouin et al., 2022) in process-based models. The reliability of data-driven models is limited by the sparse and uneven distribution of flux tower measurements and by the underlying statistical methods used to build them (Jung et al., 2020). While not perfect, process-based and data-driven models provide satisfactory results for capturing large-scale patterns compared to e.g. satellite estimations (Wang et al., 2023). This makes them valuable complementary tools to observational data.

Most recent studies examining the influence of climate on the temporal dynamics of European forest CO<sub>2</sub> fluxes rely on case studies and primarily focus on spring and summer conditions (Smith et al., 2020; Thompson et al., 2020; van der Woude et al., 2023). However, a more comprehensive assessment is needed across the entire annual cycle, as CO<sub>2</sub> release during fall and winter is expected to increase under climate change. Additionally, climate conditions vary significantly between northern and southern Europe, necessitating a broader spatial perspective. These objectives are addressed at the monthly timescale, which is considered sufficiently fine to capture both the CO<sub>2</sub> flux annual cycle and its interannual variability.

This study addresses these gaps by investigating the impact of climate on both the annual cycle and interannual variability of CO<sub>2</sub> fluxes in European evergreen needleleaf (ENF) and deciduous broadleaf forests (DBF). Using ICOS network observations alongside state-of-the-art data-driven and process-based model estimates, we first characterize the observed annual cycle and interannual variability of CO<sub>2</sub> fluxes across Europe. We then evaluate model performance in capturing the temporal phasing and magnitude of these fluxes at the site scale. Finally, we assess the influence of climate on both seasonal and interannual CO<sub>2</sub> flux variations, leveraging the extended temporal coverage provided by models.

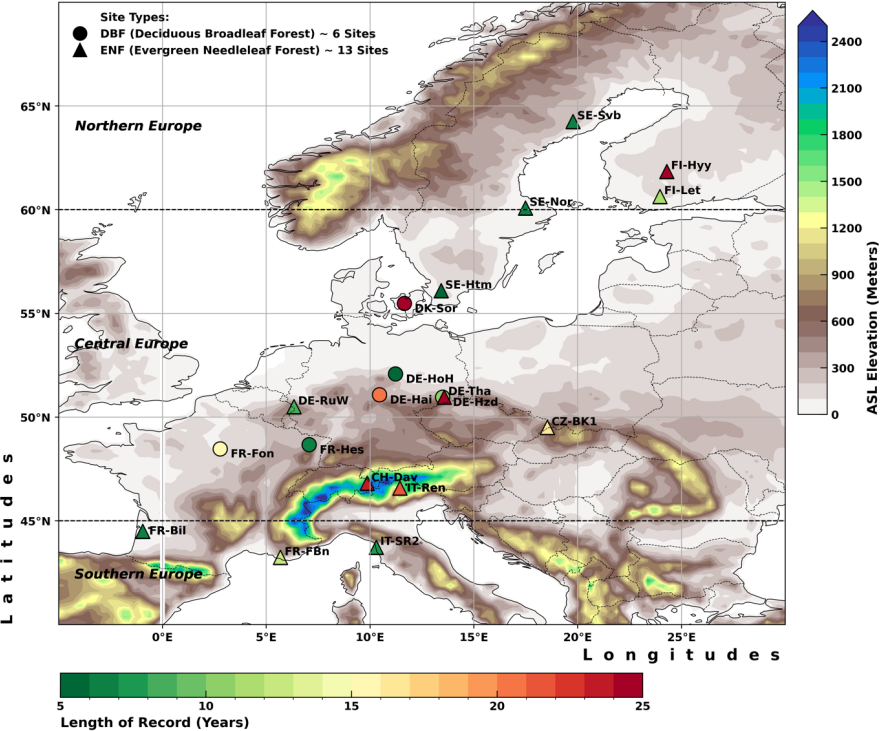
## 2 Materials & Methods

### 2.1 Site description

a supprimé: s



201 Out of the 24 ENF and DBF sites from the ICOS network, we selected the 19 sites (Fig. 1), 13 classified as ENF  
 202 and 6 as DBF, for which observed CO<sub>2</sub> fluxes are available for at least 5 years (Table 1). These sites allow to  
 203 sample the different climatic zones of Europe. Three ENF sites (FR-Bil, FR-FBn and IT-SR2) are located in the  
 204 northern region of southern Europe, close to 45°N, and ranging from sea level to 400 m in elevation. They are  
 205 characterized by mild, wet winters and hot dry summers, with annual mean temperature and precipitation of 12.9–  
 206 13.90 °C and 700–960 mm, respectively. Four ENF sites (FI-Hyy, FI-Let, SE-Nor and SE-Svb) are located in  
 207 northern Europe (60–65°N) at an elevation below 270 m. They are characterized by subarctic climate with annual  
 208 mean temperature and precipitation of 1.8–6.5 °C and 586–711 mm, respectively. The remaining twelve sites (6  
 209 DBFs and 6 ENFs) are situated in central Europe within the 45–60°N, 2.5–20°E domain, encompassing a wide  
 210 range of elevations (40–1730 m) and spanning temperate to continental climates. As a result, they exhibit  
 211 substantial variability in annual mean temperature (4.3–11.4 °C) and precipitation (563–1338 mm).  
 212



213 **Figure 1.** Location of the CO<sub>2</sub> flux measurement sites from the FLUXNET network across Europe selected for  
 214 this study. The symbol “●” corresponds to the 6 sites located in Deciduous Broadleaf Forest (DBF) while the  
 215 symbol “▲” indicates the 13 sites located in the Evergreen Needleleaf Forests (ENF). The vertical colour scale  
 216 represents the terrain height (ASL) in meters. The horizontal colour scale indicates the length of the CO<sub>2</sub> flux  
 217 record for each site. The elevation layer comes from National Geophysical Data Center/NESDIS/NOAA/U.S.  
 218 Department of Commerce (1995): TerrainBase, Global 5 Arc-minute Ocean Depth and Land Elevation from the  
 219 US National Geophysical Data Center (NGDC), <https://doi.org/10.5065/E08M-4482>. Distributed under CC by 4.0.  
 220  
 221  
 222

Table 1. European FLUXNET sites examined in this study.

Site Name	Site ID	Latitude (°North)	Longitude (°East)	Elevation (Meters)	Land cover	Period of record	Length of record (Years)	MAT (°C)	MAP (mm)
<i>Northern Europe (Above 60°N)</i>									
Svartberget	SE-Svb	64.25611	19.7745	267	ENF	2014/01 – 2020/12	7	1.8	614.0
Hyttiala	FI-Hyy	61.8474	24.2948	181	ENF	1996/01 – 2020/12	25	3.5	711.0
Lettosuo	FI-Let	60.6418	23.9595	111	ENF	2009/01 – 2020/12	12	4.6	627.0
Norunda	SE-Nor	60.0865	17.4795	45	ENF	2014/01 – 2020/12	7	6.5	586.0
<i>Central Europe (45°N – 60°N)</i>									
Hyltemossa	SE-Htm	56.09763	13.41897	115	ENF	2015/01 – 2020/12	6	7.4	707.0
Soroe	DK-Sor	55.4859	11.6446	40	DBF	1996/01 – 2020/12	25	9.0	640.0
Hohes Holz	DE-HoH	52.08656	11.22235	193	DBF	2015/01 – 2020/12	6	9.1	563.0
Hainich	DE-Hai	51.0792	10.4522	430	DBF	2000/01 – 2020/12	21	8.3	744.0
Hetzdorf	DE-Hzd	50.96381	13.48978	395	DBF	2010/01 – 2020/12	11	7.6	877.0
Tharandt	DE-Tha	50.9626	13.5651	385	ENF	1996/01 – 2020/12	25	8.1	829.0
Wustebach	DE-RuW	50.50493	6.330962	610	ENF	2012/01 – 2020/12	9	7.5	1250.0
Bily Kriz	CZ-BK1	49.5021	18.5369	875	ENF	2004/01 – 2020/12	17	6.2	1338.1
Hesse	FR-Hes	48.6741	7.06465	310	DBF	2014/01 – 2020/12	7	10.0	889.0
Fontainebleau- Barbeau	FR-Fon	48.4764	2.7801	103	DBF	2005/01 – 2020/12	16	11.4	678.9
Davos	CH-Dav	46.8153	9.8559	1639	ENF	1997/01 – 2020/12	24	4.3	876.0
Renon	IT-Ren	46.5869	11.4337	1730	ENF	1991/01 – 2020/12	22	4.9	970.8
<i>Southern Europe (Below 45°N)</i>									
Bilos	FR-Bil	44.49365	– 0.95609	39	ENF	2014/01 – 2020/12	7	12.9	960.1
San Rossore 2	IT-SR2	43.732	10.2909	4	ENF	2013/01 – 2020/12	8	15.3	950.0
Font-Blanche	FR-FBn	43.24079	5.67865	436	ENF	2008/01 – 2020/12	13	13.9	700.0

Columns 1–5 provide information on the site, including its name, ID, latitude, longitude, and elevation. Columns 6–8 describe the land cover classification, the period of available records, and the record length for each FLUXNET site. Columns 9–10 present the site's mean annual climatic characteristics, including temperature (MAT) and precipitation (MAP).

2.2 Carbon flux data

2.2.1 Observations

Measured CO<sub>2</sub> fluxes come from the Warm Winter 2020 (Team and Centre, 2022), an update of the FLUXNET2015 dataset (Pastorello et al., 2020) available on the ICOS platform (<https://www.icos-cp.eu/data-products>). For each site, we selected daily time series of NEE (NEE\_VUT\_REF), GPP (GPP\_DT\_VUT\_REF) and RECO (RECO\_DT\_VUT\_REF), the latter two fluxes being derived from the daytime flux partitioning method (Lasslop et al., 2010). Preliminary analyses show weak impact of the partitioning method (not shown).

The temporal coverage of the data varies by site (Table 1): less than 10 years for eight sites (SE-Svb, SE-Nor, SE-Htm, DE-HoH, DE-RuW, FR-Hes, FR-Bil, and IT-SR2), between 10 and 20 years for five sites (FI-Let, DE-Hzd, CZ-BK1, FR-Fon, and FR-FBn), and more than 20 years for six sites (FI-Hyy, DK-Sor, DE-Hai, DE-Tha, CH-Dav, and IT-Ren). Given these limitations, the observational dataset likely lacks sufficient temporal depth to robustly assess the impact of climate on tower CO<sub>2</sub> flux interannual variability, highlighting the usefulness of models as complementary tools.

## 2.2.2 Data-driven models

Four data-driven models are used in this study (Table 2). The first data-driven model has been developed by the CarbonSpace company, to quantify carbon exchange at the site-scale by integrating remote sensing data, meteorological variables, and eddy-covariance flux measurements. A lagrangian particle dispersion model is used for footprint gas attribution. A machine learning model is used to solve the non-linear regression problem of estimating fluxes from remote sensing and meteorological variables (Zhuravlev et al., 2022). For this study, the learning method was updated from the kernel method used in Zhuravlev et al. (2022) to an ensemble tree method (Chen and Guestrin, 2016). The key advantages of the CarbonSpace model include its scalability, high spatial resolution, and improved prediction accuracy through robust data quality control and advanced machine learning techniques. CarbonSpace provides monthly NEE only but at a very high spatial resolution (few hectares) from 01-2000 to 08-2023. This allows to get as close as possible to the 19 sites (around 1.8 ha centered on each tower) and their associated CO<sub>2</sub> flux measurement footprints.

The ~~three other~~ data-driven models come from the FLUXCOM initiative (Tramontana et al., 2016; Jung et al., 2019; Jung et al., 2020; Nelson et al., 2024). ~~The first two are~~ a 3-member ensemble forced by both ERA5 reanalysis (Hersbach et al., 2020) and satellite data from the Moderate Resolution Imaging Spectroradiometer (MODIS), and a 9-member ensemble forced by MODIS only. The members differ by the machine learning method used to build each of the two models detailed in Jung et al. (2019). These models, named FLUXCOM-ERA5 and FLUXCOM-MODIS hereafter, provide global maps of monthly NEE, GPP and RECO derived with a daytime partitioning. The FLUXCOM-ERA5 model has a coarser resolution (0.5° x 0.5°) than the FLUXCOM-MODIS (0.08° x 0.08°) but covers a longer period (1979-2018 versus 2001-2015). ~~The last model, FLUXCOM-X, is a 1-member model improving the coverage and quality of the training, as well as satellite data processing, and providing CO<sub>2</sub> fluxes at higher spatial resolution (0.05° x 0.05°) and for a longer period (2001-2020).~~

The four data-driven models include most, if not all, ICOS sites mobilised in this study. They accurately capture the mean annual and seasonal cycles of CO<sub>2</sub> fluxes (Tramontana et al., 2016; Jung et al., 2020; He et al., 2022; Zhuravlev et al., 2022) and are expected to outperform process-based models since the latter do not ~~directly~~ assimilate observed CO<sub>2</sub> fluxes. The methodological framework (e.g., machine learning model, forcing data and horizontal resolution) remains different between the data-driven models.

**a supprimé:** . The CarbonSpace model is designed

**a supprimé:** second and third

**a supprimé:** and have been retrieved from the data portal of the Max Planck Institute for Biochemistry (<https://www.bgc-jena.mpg.de>)

**a supprimé:** . The FLUXCOM models use eddy-covariance data from 224 flux-tower sites from the FLUXNET La Thuile dataset (<http://fluxnet.fluxdata.org/data/la-thuille-dataset/>) and the CarboAfrica network (Valentini et al., 2014). Among the various models available, we retained two models:

**a supprimé:**

**a mis en forme :** Indice

**a supprimé:** An inter-model convergence will be interpreted as a forced response imposed by the observations. A divergence will be interpreted as uncertainties induced by the methodological framework.

294 **Table 2.** Data-driven and process-based models used in this study.  
295

Type and Name of the Dataset	Ensemble Members	Temporal and Spatial Resolution	Temporal Coverage Available	Description	References
Data-driven models					
CarbonSpace	1	Monthly ~ Hectometric	01/2000 – 08/2023	Data-driven models trained using FLUXNET observations	Zhuravlev et al., (2022)
FLUXCOM-ERA5	3	Monthly / ~ 50 km	01/1979 – 12/2018		Jung et al. (2019, 2020); Tramontana et al. (2016)
FLUXCOM-MODIS	9	Monthly / 0.08° (~8 km)	01/2001 – 12/2015		Jung et al. (2019, 2020)
FLUXCOM-X-BASE	1	Monthly / 0.05° (~5 km)	01/2001 – 12/2021		Nelson et al. (2024)
Process-based models					
SMAP-L4C	1	Daily / ~ 9 km	03/2015 – 09/2023	Reanalysis assimilated satellite-derived soil moisture	Jones et al. (2017); Kimball et al. (2022)
TRENDY	15	Monthly / 0.5° and coarser depending on the model	Since 1700	Dynamic Global Vegetation Models (S3 simulation forced by time-varying CO <sub>2</sub> , climate and land use observations)	Friedlingstein et al. (2023); Sitch et al. (2024)
Column 1 specifies the model type and name. Columns 2–4 detail the number of members in each dataset, the space-time resolution, and the period of output availability. Columns 5–6 provide a brief description of each dataset along with references.					

296  
297  
298 **2.2.3 Process-based models**  
299

300 Two process-based models are considered (Table 2): the SMAP (Soil Moisture Active Passive) Level 4 Carbon  
301 model (SMAP-L4C hereafter) and an ensemble of Dynamic Global Vegetation Models (DGVM) from the  
302 TRENDY project (<https://sites.exeter.ac.uk/trendy>). The SMAP-L4C product is produced operationally by the  
303 NASA SMAP mission. It can be considered as a reanalysis product since it uses the Goddard Earth Observing  
304 System version 5 (GEOS-5) land model to assimilate SMAP L-band microwave observations and is forced with  
305 observed land cover and vegetation from the Moderate Resolution Imaging Spectroradiometer (MODIS) and  
306 Visible Infrared Imaging Radiometer Suite (VIIRS). The global processing is conducted on 1 km sub-grids using  
307 spatially aggregated MODIS PFTs and VIIRS fPAR inputs, allowing to distinguish up to eight individual plant  
308 functional types (PFTs) within each 9 km × 9 km product grid cell. However, the model processing uses coarser  
309 spatial resolution (9 km and 0.25 degree) daily inputs from the SMAP L4 soil moisture (L4\_SM) and GMAO  
310 Forward Processor (FP) surface meteorology. Among other variables, the SMAP-L4C outputs provide daily NEE  
311 and GPP (RECO deduced from the difference between NEE and GPP) in a consistent global grid from March 2015  
312 to September 2023 for each PFT, including DBFs and ENFs (Jones et al., 2017; Kimball et al., 2022). The 1-km  
313 PFT subclass distinction allows the differentiation of ENF and DBF. The L4C product is derived using coupled  
314 photosynthetic light-use efficiency and soil organic matter decomposition models to estimate daily NEE and its  
315 component carbon fluxes, where GPP is reduced from PFT-specific optimal rates for unfavourable daily climate  
316 conditions, including cold temperatures, low light levels, excessive atmospheric vapour pressure deficits and low

317 root zone (0-1m depth) soil moisture levels defined from SMAP L4\_SM and GMAO FP meteorology. The  
 318 associated product quality assessment report gives details of the model algorithms and the calibration, validation,  
 319 and performance of the L4C version 7 product used in this study (Endsley et al., 2023).

320  
 321 In addition to SMAP-L4C, this study also uses outputs from 15 Dynamic Global Vegetation Models (DGVMs) of  
 322 the Trends and Drivers of Regional-Scale Terrestrial Sources and Sinks of Carbon Dioxide (TRENDY version 12)  
 323 project. These models are routinely mobilised to assess global carbon budget trends and for attributing changes to  
 324 CO<sub>2</sub>, climate and land use (Friedlingstein et al., 2023; Sitch et al., 2024). Appendix Table 1 provides the list of the  
 325 15 DGVMs used in this study. Here, we used outputs from the S3 scenario, with simulations starting in 1700 and  
 326 forced by time-varying observed CO<sub>2</sub>, climate and land use change. All simulations have horizontal resolution of  
 327 0.5° x 0.5° and monthly outputs.

328  
 329

#### 330 2.2.4 Climate data

331  
 332 To investigate the impact of climate on CO<sub>2</sub> fluxes, we use the ERA5-Land dataset (Muñoz-Sabater et al., 2019)  
 333 produced by the European Centre for Medium-Range Weather Forecasts (ECMWF). This dataset results from the  
 334 ECMWF land surface model (HRESSEL) operating at 0.1° spatial resolution and forced by the ERA5 reanalysis  
 335 (Hersbach et al., 2020). This product provides hourly outputs for land surface, hydrological and meteorological  
 336 variables from 1950 onwards. In this study, we use incident shortwave radiation, temperature at 2 m (T<sub>2m</sub>) and  
 337 averaged soil moisture (SM<sub>AVG</sub>). We use the volumetric soil water content averaged across the 4 available soil  
 338 layers (0–7 cm, 7–28 cm, 28–100 cm, and 100–289 cm). Since it accounts for both liquid water and ice, this  
 339 parameter remains above zero even when temperatures drop below freezing. Results obtained with incident  
 340 shortwave radiation show no clear seasonality in correlation patterns with NEE, suggesting that greater light  
 341 availability generally enhances CO<sub>2</sub> sequestration. For this reason, we do not include results for this variable in  
 342 the main analysis. We also use relative humidity together with T<sub>2m</sub> to compute the air vapour pressure deficit  
 343 (VPD), an integrative metric accounting for both heat and water stress effects (Carrara et al., 2004; von Buttlar et  
 344 al., 2018; Kong et al., 2022; van der Woude et al., 2023). The VPD is defined as the difference between the amount  
 345 of moisture that is actually in the air and the amount of moisture that air could hold at saturation. The VPD is  
 346 computed using the Tetens formula (Monteith and Unsworth, 2007) following Eq. (1):

347  
 348 
$$VPD = \left(1 - \frac{HU}{100}\right) * \text{saturation vapor pressure} = \left(1 - \frac{HU}{100}\right) (610.78 * \exp(\frac{T}{T+237.3} * 17.2694)) \quad (1)$$

349  
 350 In the end, three ERA5-Land climate variables (T<sub>2m</sub>, SM<sub>AVG</sub> and VPD) are used to assess the impact of climate on  
 351 the annual cycle and interannual variability of CO<sub>2</sub> fluxes. These variables capture the influence of thermal,  
 352 hydrological, and atmospheric moisture demand conditions on CO<sub>2</sub> flux dynamics.

353  
 354  
 355

**a supprimé:** use the average of the four ERA5-Land soil moisture  
**a supprimé:** , representing the volumetric soil water content at different depths

**a supprimé:** and T<sub>2m</sub> lead to similar results. We therefore show the results for T<sub>2m</sub> only

362 **2.3 Methodology**

363

364 For the gridded datasets (ERA5-Land, FLUXCOM, TRENDY, and SMAP-L4C), we extracted the nearest grid  
365 point to each flux tower site. Note that SMAP-L4C simulates spurious CO<sub>2</sub> fluxes at the DE-Hzd site. Therefore,  
366 this site is not included in the analysis for this model. Since these datasets have varying temporal resolutions  
367 (Tables 1 and 2), all were aggregated to a monthly timescale. From these monthly values, we computed the mean  
368 annual cycle by averaging all available years in each dataset, along with interannual variability, defined by the  
369 standard deviation and coefficient of variation.

370

371 Model skill in capturing observed CO<sub>2</sub> flux variability is evaluated over overlapping periods between each model  
372 and observation. The number of overlapping years varies significantly across model–observation pairs (Fig. 2a).

373 *Two complementary metrics are used for model evaluation: the bias (model minus observation), which assesses*  
374 *errors in magnitude, and the Bravais-Pearson correlation coefficient (R), which evaluates temporal co-variability.*

375 *These metrics capture distinct aspects of model performance and are not necessarily correlated.* For the annual  
376 cycle, we computed monthly biases for each overlapping year and present the mean bias averaged across all months  
377 and years. Model skill in reproducing the seasonal timing of CO<sub>2</sub> fluxes is assessed by correlating the 12 monthly  
378 modelled and observed values within each overlapping year, with the multi-year mean R reported. Correlations  
379 are considered significant at the 95% confidence level if the mean p-value is below 0.05. For interannual  
380 variability, biases are calculated as the difference between modelled and observed standard deviations for each  
381 month. Co-variability between observed and modelled CO<sub>2</sub> fluxes is assessed only for model-observation pairs  
382 with at least 10 overlapping years, ensuring robust signal detection. Correlations were deemed significant when p  
383 < 0.05.

384

385 The impact of climate on CO<sub>2</sub> fluxes is assessed for overlapping years between each CO<sub>2</sub> flux dataset and ERA5-  
386 Land. The number of overlapping years varies widely across datasets (Fig. 2b), ranging from low coverage in  
387 observations and SMAP-L4C to over 70 years in TRENDY. The correlation coefficient (R) was used to assess  
388 climate impacts, with the mean R reported for the annual cycle and individual R values for interannual variability.

389

390 To ensure results were not driven by long-term trends, analyses have been conducted using both raw and detrended  
391 climate time series (not shown), yielding similar outcomes. Additionally, for observed CO<sub>2</sub> fluxes, we verified  
392 ERA5-Land climate data reliability by comparing results with observed climate measurements from the  
393 FLUXNET database (not shown).

394

395 For conciseness, we primarily present results using the ensemble mean of FLUXCOM (ERA5 and MODIS) and  
396 TRENDY models. However, uncertainties arising from machine learning methods and DVGM physical  
397 parameterizations are discussed in the model evaluation section.

398

**a supprimé:** Magnitude and co-variability errors are assessed using bias and the

**a supprimé:** , respectively

**a supprimé:**

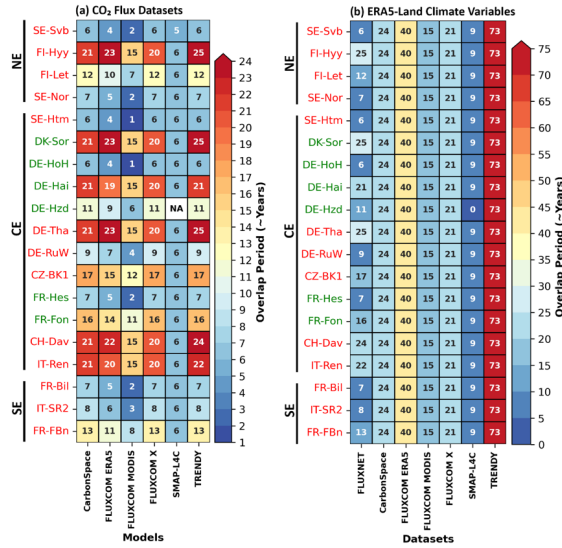
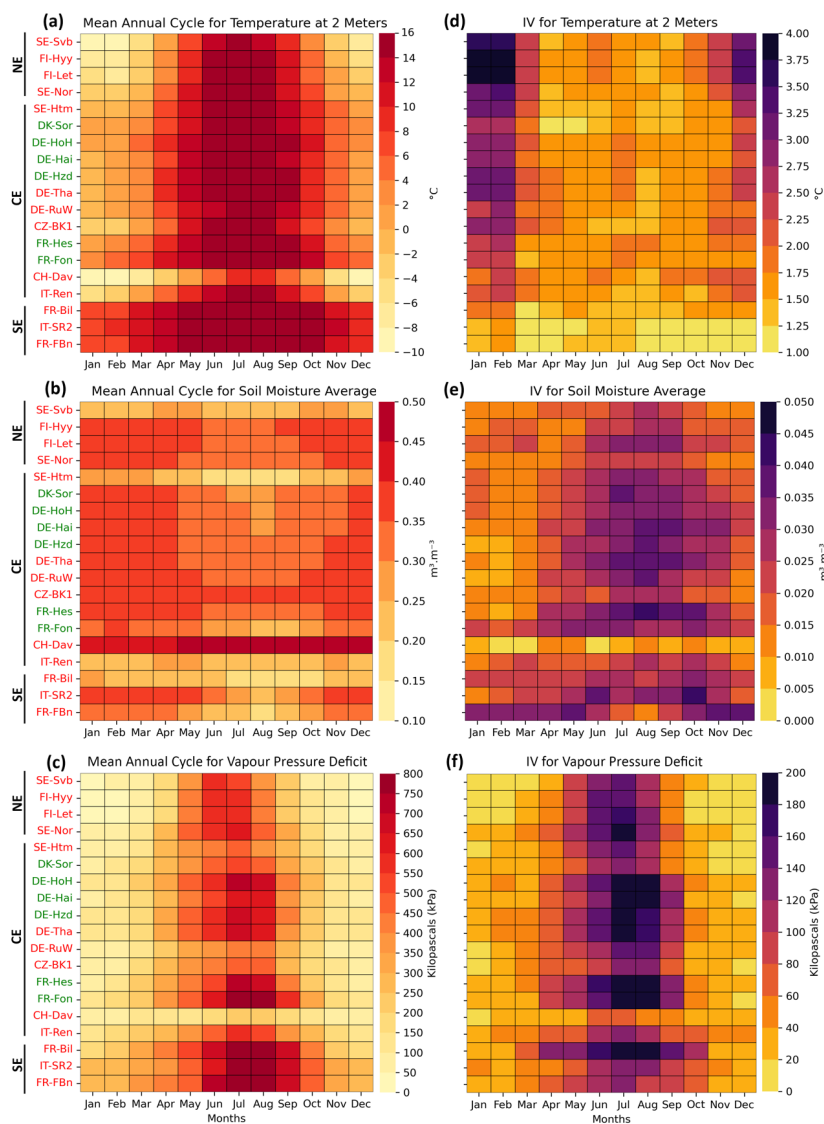


**Figure 2.** Number of overlapping years between (a) observed and modelled CO<sub>2</sub> fluxes, and (b) ERA5-Land climate and observed and modelled CO<sub>2</sub> fluxes. The overlapping periods in panel (a) are used to assess the model's ability to capture the annual cycle and interannual variability of CO<sub>2</sub> fluxes. In panel (b), the overlapping periods are used to evaluate the co-variability between CO<sub>2</sub> fluxes and the annual cycle and interannual variability of ERA5-Land climate. ENF sites are displayed in red text, while DBF sites are highlighted in green. Sites are ordered from north to south based on their latitude, with black vertical lines indicating the boundaries between northern (NE), central (CE) and southern (SE) Europe.

### 3 Results

#### 3.1 Observed climate and CO<sub>2</sub> fluxes mean annual cycle and interannual variability

Figure 3 shows the mean annual cycle and interannual variability of T<sub>2m</sub>, SM<sub>AVG</sub> and VPD associated with each site. Overall, all sites depict higher T<sub>2m</sub> and VPD and lower SM in summer than in winter (Figs. 3a-c). A south-north gradient is evident, with more marked annual amplitude and shorter summer in northern than southern Europe. Few sites deviate from this pattern, including e.g., the Alpine site (CH-Dav), which depicts relatively cold and wet conditions, as well as low VPD, all year long. While the interannual variability of T<sub>2m</sub> is the largest in winter regardless of the site, it increases markedly from south to north (Fig. 3d). The reverse is found for VPD, with higher interannual variability in summer than winter, especially south of 60°N (Fig. 3f). The interannual variability in SM<sub>AVG</sub> (Fig. 3e) is low all year long in the Alpine site, relatively low in northern Europe, high from spring to summer in the mid-latitudes and in fall and winter in the Mediterranean region (FR-FBn).



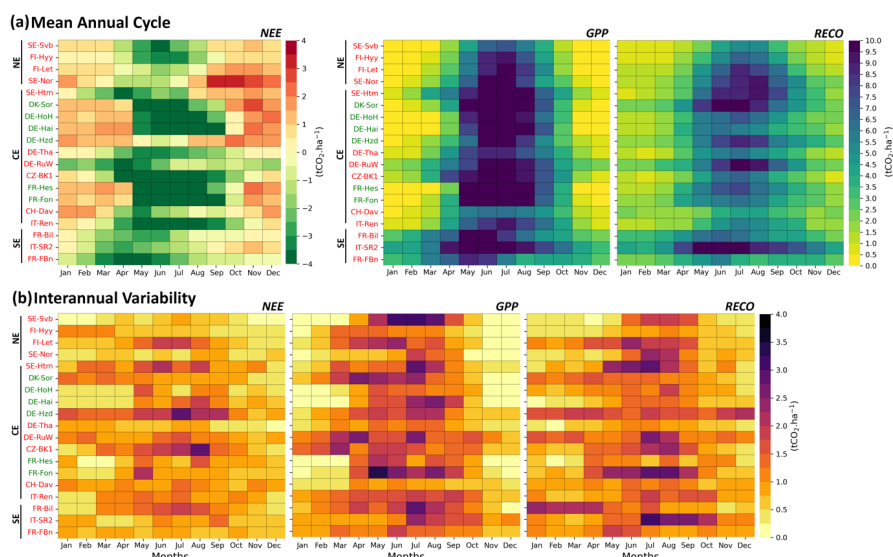
**Figure 3. (a-c)** Mean annual cycle and **(d-f)** interannual variability (*i.e.*, **IV**) in monthly 2 m air temperature ( $T_{2m}$ ), soil moisture ( $SM_{avg}$ ), and vapour pressure deficit (VPD), respectively, for each study site for the 1979–2023 period. Climate conditions at each site are extracted from the nearest grid point of the  $9\text{ km} \times 9\text{ km}$  ERA5-Land product. ENF sites are displayed in red text, while DBF sites are highlighted in green. Sites are ordered from north to south based on their latitude, with black vertical lines indicating the boundaries between northern (NE), central (CE) and southern (SE) Europe.



Figure 4a displays the mean annual cycle of monthly NEE, GPP and RECO as provided by FLUXNET observations. The mean annual cycle in NEE is not necessarily phased on that of GPP and RECO, the two latter reaching their highest values from May to August in most sites. Significant differences are found between northern (SE-Nor, FI-Let, FI-Hyy and SE-Svd) and southern (FR-FBn, IT-SR2 and FR-Bil) Europe, where ENF sites only are available. The annual cycle is more marked and the sequestration period (i.e., month associated with negative NEE values) is shorter in the former than the latter region. Temperature conditions (and light availability) are the main drivers explaining these differences. In central Europe, where both ENF and DBF sites are available, there is a clear impact of land cover class. The DBF sites show pronounced annual cycle with strong CO<sub>2</sub> uptake (below -3 tCO<sub>2</sub>.ha<sup>-1</sup>) from May to August, and up to some extent in September, and strong CO<sub>2</sub> release the remaining months (above 2 tCO<sub>2</sub>.ha<sup>-1</sup>). Conversely, the ENF sites show smoothed annual cycle: the summer peak of CO<sub>2</sub> sequestration barely exceeds -3 tCO<sub>2</sub>.ha<sup>-1</sup> and the winter peak of CO<sub>2</sub> release rarely exceeds 1 tCO<sub>2</sub>.ha<sup>-1</sup>. Two sites deviate from the general pattern: the DE-Hzd DBF site, which acts as a CO<sub>2</sub> source nearly year-round, and the DE-RuW ENF site, which remains a consistent CO<sub>2</sub> sink on average.

The interannual variability of NEE, GPP, and RECO, as defined by the standard deviation metric, tends to be stronger during the growing season (spring to fall) than in winter at almost all sites (Fig. 4b). The exact pattern depends on the CO<sub>2</sub> flux, site and land cover class considered. GPP is always close to zero during winter in DBF sites since trees are not photosynthetically active. This is not the case for ENF sites, particularly those located in central Europe (DE-RuW and CZ-BK1). The interannual variability of RECO is substantial in summer only in northern Europe. However, it can be non-negligible in other seasons in central and southern Europe. There, significant differences between geographically close sites (e.g., FR-Bil and IT-SR2) suggest additional drivers such as soil properties. The interannual variability of NEE is (i) weaker than that of GPP and RECO, likely due to the strong coupling between GPP and RECO, (ii) primarily driven by RECO in winter and (iii) a complex response of GPP and RECO in the remaining seasons. Note that the pattern of CO<sub>2</sub> flux interannual variability depends on the metric used to assess it. When defined using the coefficient of variation, interannual variability is low in summer and high in winter for GPP and RECO, with increasing variability toward the north. For NEE, variability remains significant throughout the year, particularly from fall to winter (Fig. A1).

Overall, the mean annual cycle of observed CO<sub>2</sub> fluxes in European forests follows a clear spatial pattern driven by climate conditions and land cover class. In contrast, the interannual variability of observed CO<sub>2</sub> fluxes exhibits greater spatial noise across Europe and depends on the metric used. Nevertheless, it remains significant, highlighting the importance of assessing the impact of climate on it throughout the annual cycle.



**Figure 4. (a)** Mean annual cycle and **(b)** interannual variability in monthly NEE, GPP and RECO (from left to right, respectively) as measured by eddy-covariance over the most extended available period for each site (see Table 1 for details). ENF sites are displayed in red text, while DBF sites are highlighted in green. Sites are ordered from north to south based on their latitude, with black vertical lines indicating the boundaries between northern (NE), central (CE) and southern (SE) Europe.

## 3.2 Model evaluation in capturing the mean annual cycle and interannual variability of CO<sub>2</sub> fluxes

### 3.2.1 Mean annual cycle

The model skill in capturing the temporal phasing of the annual cycle and the magnitude in observed CO<sub>2</sub> fluxes is assessed in terms of correlation and mean bias, respectively (see section 2.3 for details). All models accurately capture the observed temporal phasing of GPP and RECO, with correlation values often above 0.8 (Fig. 5a). The model skill is poorer but still correct for NEE, with correlation values remaining above 0.6 for most sites and models. The weaker correlation found for NEE compared to GPP and RECO is not surprising, as accurately estimating the NEE annual cycle requires precise estimation of both the temporal phasing and magnitude of GPP and RECO.

a supprimé: observed

a supprimé: the

a supprimé: observed annual cycle

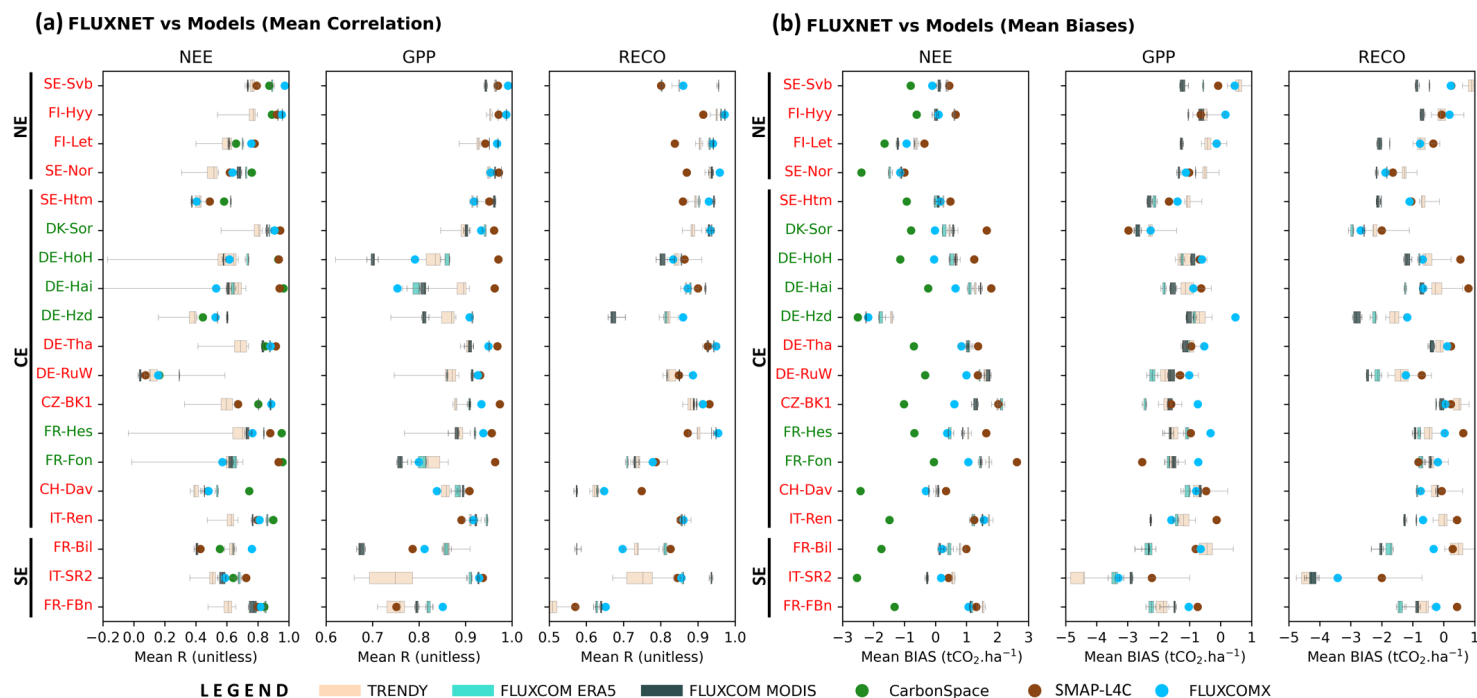


**Figure 5.** Model skill in capturing (a) the annual cycle and (b) magnitude of observed NEE, GPP and RECO. The model skill in capturing the annual cycle is assessed through the Bravais-Pearson correlation coefficient (R) calculated between the simulated and observed annual cycle of monthly CO<sub>2</sub> fluxes (12 values) for each year of the overlapping period. The multi-year mean R values are shown. The magnitude error is computed as the difference between simulated and observed CO<sub>2</sub> fluxes (model minus observation) for each month of the overlapping period. The mean magnitude error is shown. Results are displayed using colored dots for single member models (CarbonSpace, FLUXCOM-X and SMAP-L4C) and boxplots for multi-member FLUXCOM models and the multi-model TRENDY ensemble. The boxes have lines at the lower quartile, median, and upper quartile values. The whiskers are lines extending from each end of the boxes to show the extent of the full range of the data, including outliers. The colour attributed to each model is detailed in the legend. ENF sites are displayed in red text, while DBF sites are highlighted in green. Sites are ordered from north to south based on their latitude, with black vertical lines indicating the boundaries between northern (NE), central (CE) and southern (SE) Europe.

Despite reasonable annual cycles, the models struggle in capturing the observed magnitude of RECO and GPP (Fig. 5b). Three groups emerge. The first group includes the FLUXCOM (ERA5, MODIS and X) and TRENDY models, which underestimate both GPP and RECO by about similar amounts, resulting in relatively “weak” positive biases in NEE. The second group corresponds to the SMAP-L4C model, which overestimates RECO by 1 tCO<sub>2</sub> ha<sup>-1</sup> month<sup>-1</sup> while underestimating GPP by the same amount, leading to a systematic underestimation of CO<sub>2</sub> sequestration by approximately 2 tCO<sub>2</sub> ha<sup>-1</sup> month<sup>-1</sup>. The last group is the CarbonSpace data-driven model, which is the only model that systematically overestimates CO<sub>2</sub> sequestration, by up to 2.5 tCO<sub>2</sub> ha<sup>-1</sup> month<sup>-1</sup>. However, the cause of this overestimation is unclear, as this model does not provide separate GPP and RECO estimates.

Figure 5 highlights key insights into model behaviour. First, the data-driven and SMAP-L4C models generally outperform the TRENDY models in capturing the annual cycle of CO<sub>2</sub> fluxes but do not necessarily provide better estimates of flux magnitude. Second, models that accurately represent the annual cycle can still struggle with magnitude. This is exemplified by the CarbonSpace data-driven model, which ranks among the best for annual cycle representation but severely overestimates CO<sub>2</sub> sequestration in many sites. Third, the machine learning methods used in the FLUXCOM-ERA and FLUXCOM-MODIS ensembles have little impact on both the annual cycle and magnitude of CO<sub>2</sub> fluxes. The input data itself appears to be more important, with the FLUXCOM models accounting for both vegetation and climate (i.e., ERA5 and X) yielding more reliable results than those accounting for vegetation alone (MODIS). Additionally, FLUXCOM-X improves upon the previous model generation for most sites. Finally, the inter-model spread within the TRENDY ensemble is much smaller for CO<sub>2</sub> flux magnitude than for temporal variability, suggesting that the primary source of uncertainty in DGVMs lies in the temporal phasing of the fluxes rather than their magnitude.

### 3.2.2 Interannual variability

We qualitatively evaluate how well the models capture the observed interannual variability of CO<sub>2</sub> fluxes in terms of magnitude (monthly bias analysis) and temporal phasing (correlation analysis) over the overlapping period of each model-observation pair.

All models strongly underestimate the magnitude in NEE interannual variability all year long (Fig. 6), particularly during summer where biases often exceed 2.5 tCO<sub>2</sub> ha<sup>-1</sup> month<sup>-1</sup>. This is a well-known bias of current data-driven and process-based models (e.g., Lin et al., 2023; Nelson et al., 2024). The only exception is the CarbonSpace model that produce weak positive or negative biases at most sites. Importantly, a biased magnitude of CO<sub>2</sub> flux interannual variability (as measured by the standard deviation) does not preclude the models to capture their temporal co-variability (as measured by correlation) with observed CO<sub>2</sub> fluxes and climate.

a supprimé: ¶

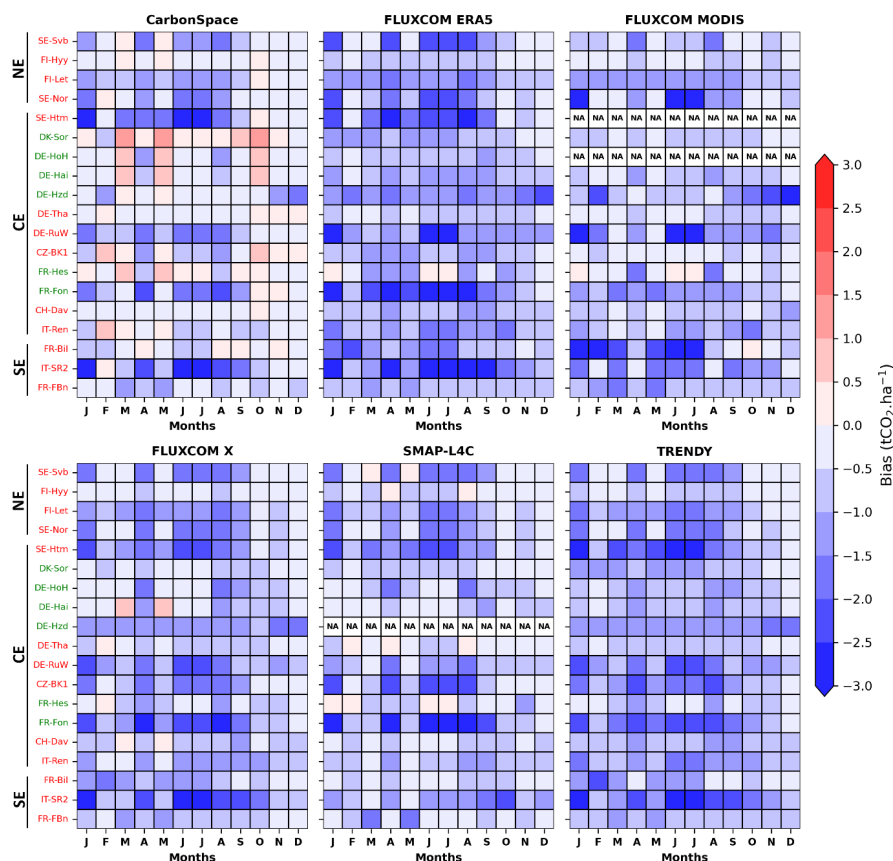


**Figure 6.** Model skill in capturing the observed magnitude in monthly NEE interannual variability. Model skill is assessed by computing biases between modelled and observed NEE interannual variability, as defined by the standard deviation of monthly fluxes. The number of years included varies depending on the model–observation pair, as shown in Fig. 2a. Cells labelled “NA” indicate cases where the overlap criterion is not met. For conciseness, biases are computed using the ensemble mean for FLUXCOM-ERA5, FLUXCOM-MODIS, and TRENDY models. ENF sites are displayed in red text, while DBF sites are highlighted in green. Sites are ordered from north to south based on their latitude, with black vertical lines indicating the boundaries between northern (NE), central (CE) and southern (SE) Europe.

Figure 7 shows the correlations between the modelled and observed interannual variability in monthly NEE. Correlation values are predominantly positive across Europe, though they are often low and not statistically significant ( $p > 0.05$ ). The correlation values tend to be higher in fall for northern Europe sites and all year long in central Europe regardless of the model. The frequent lack of statistical significance in correlations can largely be attributed to the limited number of overlapping years. This is further supported by the fact that, except for Davos, correlation values tend to be higher and more likely to reach the 95% confidence level in model–observation pairs with a greater number of overlapping years (e.g., DK-Sor, DE-Hai and DE-Tha). Another challenge in capturing

the observed temporal phasing of NEE interannual variability is that it requires accurately simulating the interannual variability of both GPP and RECO. The latter is generally better represented by models than NEE variability itself (compare Fig. 7 with Figs. A2–A3). Scale inconsistencies may also contribute to the discrepancies. While flux tower observations reflect local variability, most models represent regional-scale fluxes (and drivers). This is supported by the CarbonSpace model, the only site-scale model used in this study, which produces more satisfactory results, with positive correlation values for almost all sites and all months.

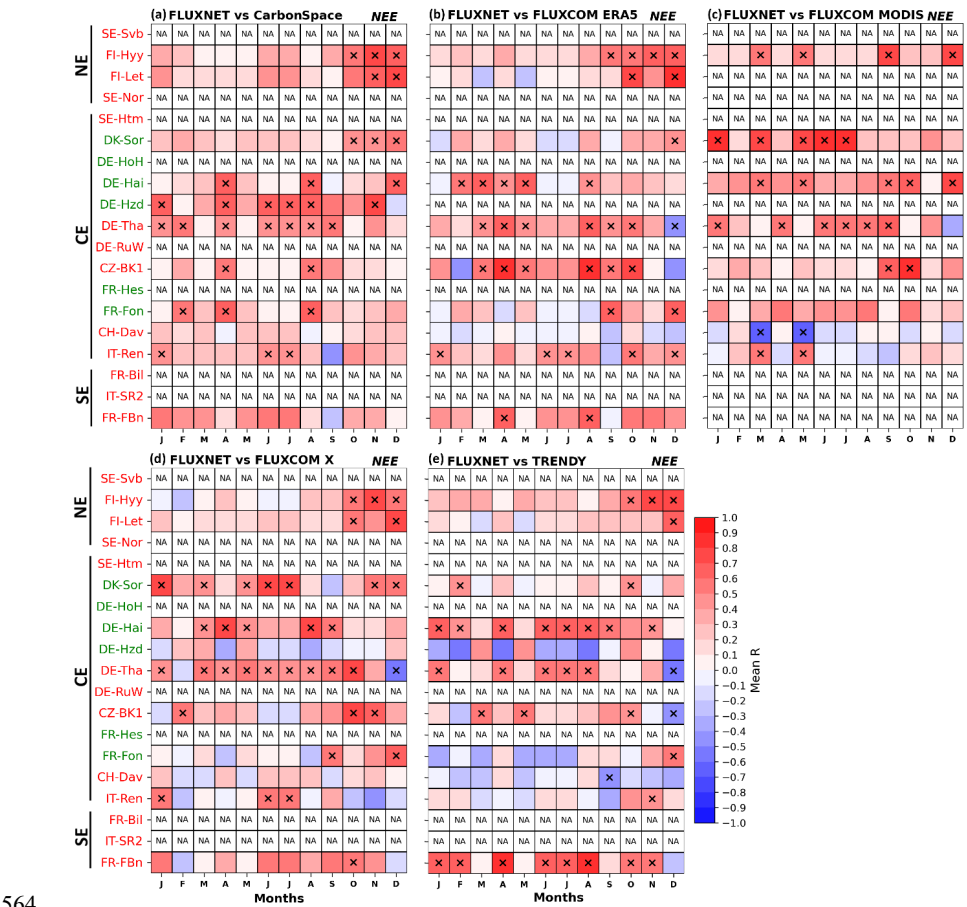


**Figure 7.** Model skill in capturing the observed temporal phasing in monthly NEE interannual variability. Model skill is assessed using the Bravais-Pearson correlation coefficient ( $R$ ), calculated using each month where at least 10 years of overlap exists between each model–observation pair. The number of years included varies depending on the model–observation pair, as shown in Fig. 2a. Correlation values marked with “x” are significant at the 95% confidence level according to the Bravais-Pearson test. Cells labelled “NA” indicate cases where the overlap criterion is not met. For conciseness, the correlation analysis is performed using the ensemble mean for FLUXCOM-ERA5, FLUXCOM-MODIS, and TRENDY models. ENF sites are displayed in red text, while DBF sites are highlighted in green. Sites are ordered from north to south based on their latitude, with black vertical lines indicating the boundaries between northern (NE), central (CE) and southern (SE) Europe.

The spread among members of the FLUXCOM ensembles is low (not shown), regardless of whether they account for climate alone or both climate and vegetation. However, Figure 7 reveals significant differences between the FLUXCOM products (ERA5, MODIS, and X; Fig. 7b–d). These differences are not necessarily due to the type of data used in these data-driven models, as the analysis periods differ between them. In contrast, the correlations between observations and the TRENDY ensemble mean (Fig. 7e) mask substantial variability among individual TRENDY models, with no single model consistently outperforming the others (Fig. A4).

These qualitative results suggest that the interannual variability of simulated NEE is at least partially aligned with that of observed CO<sub>2</sub> fluxes, supporting the use of models to assess the impact of climate on CO<sub>2</sub> flux interannual variability.

### 3.3 Climate – CO<sub>2</sub> flux relationship

#### 3.3.1 Annual cycle

Figure 8 assesses the co-variability between the annual cycle of CO<sub>2</sub> fluxes and climate variables ( $T_{2m}$ ,  $SM_{AVG}$ , and VPD) through correlation analysis. For conciseness, correlations are computed using the ensemble mean of CO<sub>2</sub> fluxes for FLUXCOM (ERA5 and MODIS) and TRENDY models. The inter-member dispersion in FLUXCOM and inter-model dispersion in TRENDY, shown in Fig. A5, are similar to those in Fig. 5 and are therefore not discussed here.

The annual cycle of CO<sub>2</sub> fluxes is closely linked to climate in both observations and models, as evidenced by statistically significant correlations at the 95% confidence level. The influence of climate on the annual cycle of CO<sub>2</sub> fluxes is generally stronger for GPP and RECO than for NEE, particularly for  $T_{2m}$  (Fig. 8a). Over Europe, GPP, RECO and CO<sub>2</sub> sequestration (i.e., negative NEE) tend to be higher when  $T_{2m}$  and VPD are high and  $SM_{AVG}$  is low. In turn, CO<sub>2</sub> fluxes are amplified in summer and damped in winter. Among the climate variables,  $T_{2m}$  and VPD exhibit stronger correlations with the CO<sub>2</sub> flux annual cycle than  $SM_{AVG}$ , reflecting their more pronounced seasonality (Fig. 3).

This climate – CO<sub>2</sub> flux relationship is particularly evident in northern and central Europe, where there is strong agreement between observations and models, as well as across different models. The only exception in central Europe is the Alpine site (CH-Dav), where  $SM_{AVG}$  is positively correlated with GPP and RECO and negatively correlated with NEE. This discrepancy arises because CH-Dav is the only site in the study where  $SM_{AVG}$  is higher in summer than in winter (Fig. 3b). In contrast, in southern Europe, the relationship between climate and NEE does not reach the 95% confidence level in observations. However, the models show a similar relationship to that found in northern and central Europe, albeit with weaker correlations. Whether this disagreement stems from the limited number of observational years available for these sites (7 to 13 years, see Table 1) or from an overestimation of climate impact on the CO<sub>2</sub> flux annual cycle remains an open question.

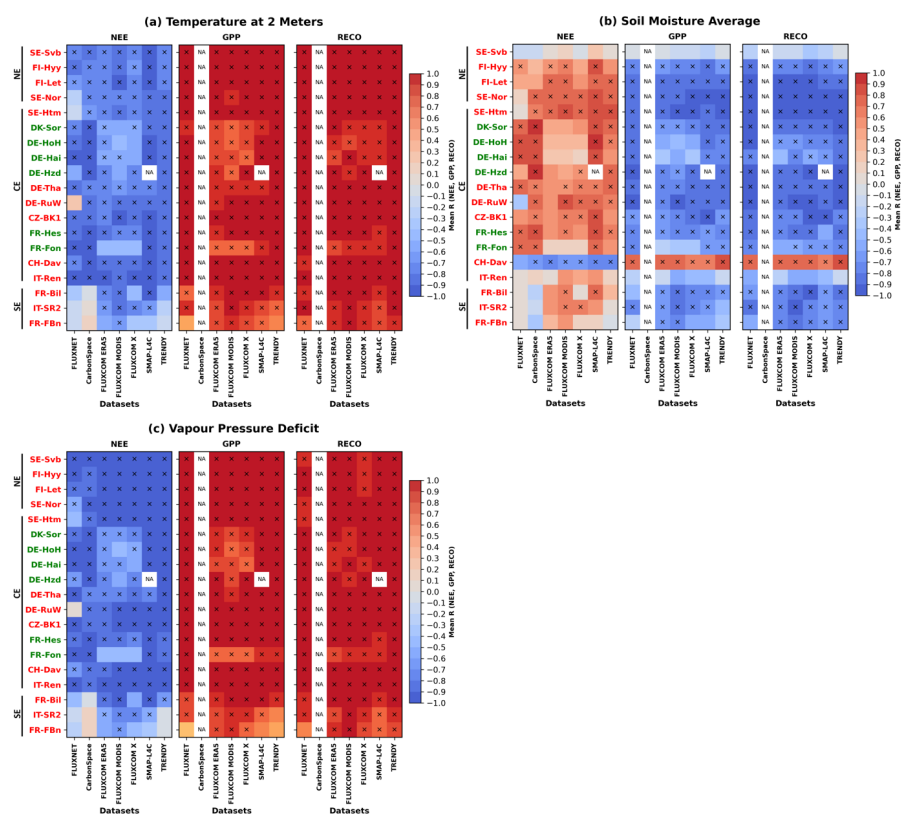


**Figure 8.** Co-variability in the annual cycle of CO<sub>2</sub> fluxes and (a) 2 m temperature, (b) soil moisture, and (c) vapour pressure deficit across all sites and datasets. Co-variability is assessed through Bravais-Pearson correlation, computed annually between CO<sub>2</sub> fluxes and ERA5-Land climate data, then averaged across years. The number of years included varies depending on the data, as shown in Fig. 2d. Correlation values marked with 'x' are significant at the 95% confidence level according to the Bravais-Pearson test. Cells labelled 'NA' indicate cases where GPP and RECO are unavailable (CarbonSpace) or where CO<sub>2</sub> flux data are corrupted (SMAP-L4C). For conciseness, correlations are computed using the ensemble mean of CO<sub>2</sub> fluxes for FLUXCOM (ERA5 and MODIS) and TRENDY models. ENF sites are displayed in red text, while DBF sites are highlighted in green. Sites are ordered from north to south based on their latitude, with black vertical lines indicating the boundaries between northern (NE), central (CE) and southern (SE) Europe.

Figure 8 also reveals differences in model behaviour. First, the climate – CO<sub>2</sub> flux relationship appears sensitive to land cover class only in data-driven models. In the FLUXCOM models (ERA5, MODIS, X), this relationship is weaker for DBFs than ENFs in central Europe, whereas the CarbonSpace model shows the opposite pattern. This sensitivity to land cover class may reflect model discrepancies, as the observed climate – CO<sub>2</sub> flux relationship does not depict such an ENF–DBF distinction. The reason for this discrepancy may involve differences in climate forcing or model spatial resolution. Second, process-based models tend to overestimate the impact of climate on the annual cycle of CO<sub>2</sub> fluxes across all sites. For example, the SMAP-L4C model amplifies the influence of T<sub>2m</sub> and S<sub>MAVG</sub> on NEE, particularly in northern Europe (Fig. 8a-b). Meanwhile, in the TRENDY models, VPD

a supprimé: remains, however, unclear, given that these data-driven models are based on the same FLUXNET sites.



636 emerges as the dominant driver of the NEE annual cycle (Fig. 8c). These results suggest that process-based models  
637 may underestimate the role of additional factors, such as soil properties, in shaping the CO<sub>2</sub> flux annual cycle.

638  
639  
640 **3.3.2 Interannual variability**

641 We now investigate the interannual co-variability between CO<sub>2</sub> fluxes and climate using correlation analysis. This  
642 is done by analyzing the full monthly timeseries of each dataset in two ways: (i) all months combined after  
643 removing the mean annual cycle and (ii) separately for each calendar month. The first approach reveals no robust  
644 relationship in the observations and weak correlations in the models (Fig. 9). In contrast, the second approach  
645 shows some consistencies in the correlation patterns across datasets, with distinct differences between  
646 northern/central Europe and southern Europe (Fig. 10). In the former region, the NEE tends to be positively  
647 correlated with T<sub>2m</sub>, SM<sub>AVG</sub> and VPD in winter and fall. This means that anomalously high T<sub>2m</sub>, VPD and SM<sub>AVG</sub>  
648 favor CO<sub>2</sub> release during the cold seasons. These patterns are similar for GPP and RECO (Figs. A6-A7), but  
649 correlations are stronger for RECO, highlighting its significant contribution to NEE interannual variability during  
650 the cold seasons. In spring (March–May), the relationship between NEE and T<sub>2m</sub>/VPD reverses compared to the  
651 cold season pattern, while that between NEE and SM<sub>AVG</sub> tends to remain positive in central Europe. In turns,  
652 anomalously high T<sub>2m</sub> and VPD, along with anomalously low SM<sub>AVG</sub> (at least in central Europe), tend to be  
653 favorable spring conditions for CO<sub>2</sub> sequestration. The increase in spring CO<sub>2</sub> sequestration under anomalously  
654 dry soil conditions is likely driven by elevated T<sub>2m</sub> and VPD, leading to enhanced evapotranspiration and drier  
655 soils. The summer pattern generally shows an opposite sign compared to spring, suggesting stronger CO<sub>2</sub>  
656 sequestration under anomalously low T<sub>2m</sub> and VPD, and high SM<sub>AVG</sub>. In southern Europe, correlation patterns are  
657 consistent across datasets in spring and summer only, showing a similar response to that observed in summer in  
658 northern/central Europe, but extended over a longer period.

a supprimé: , with a particular focus on how this relationship evolves throughout the annual cycle. Figure 9

a supprimé: illustrates the interannual relationship between climate and NEE for each month through correlation analysis.

a supprimé: The relationship is notably noisier in the observations compared to the models, due to the limited observational record and site-specific variations in measurement periods, and highlights model sensitivity. Nonetheless, the general pattern remains consistent

a supprimé: showing

a supprimé: .

a supprimé: ¶

a supprimé: ¶

a mis en forme : Indice

a supprimé: is

a supprimé: is

a supprimé: meaning that

a supprimé: low

a supprimé: and

a supprimé: promote

a mis en forme : Indice

a supprimé:

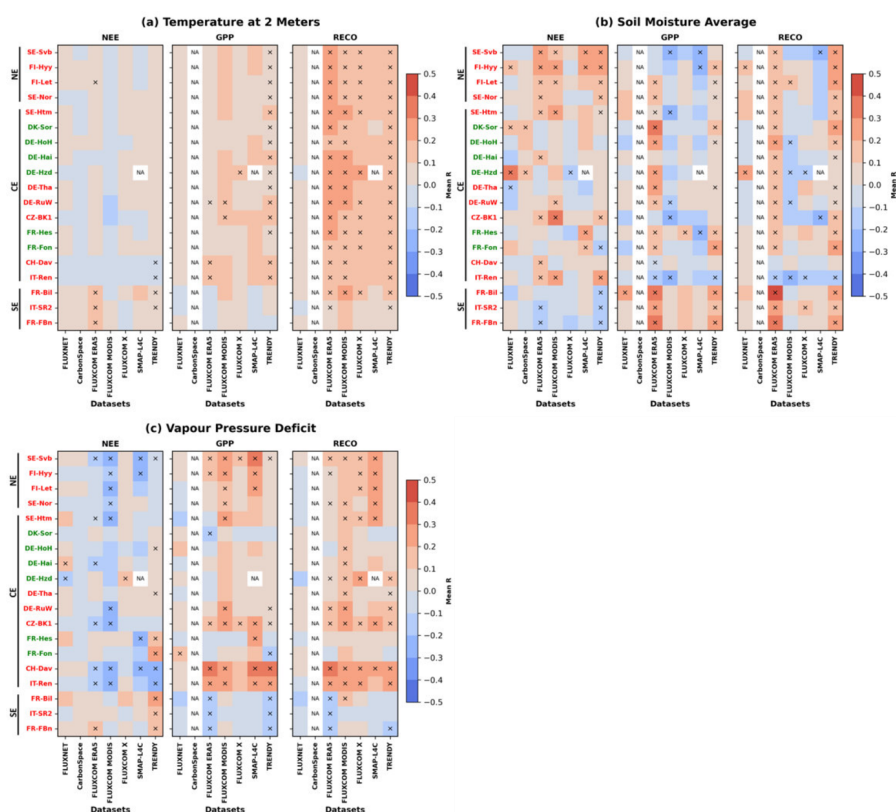
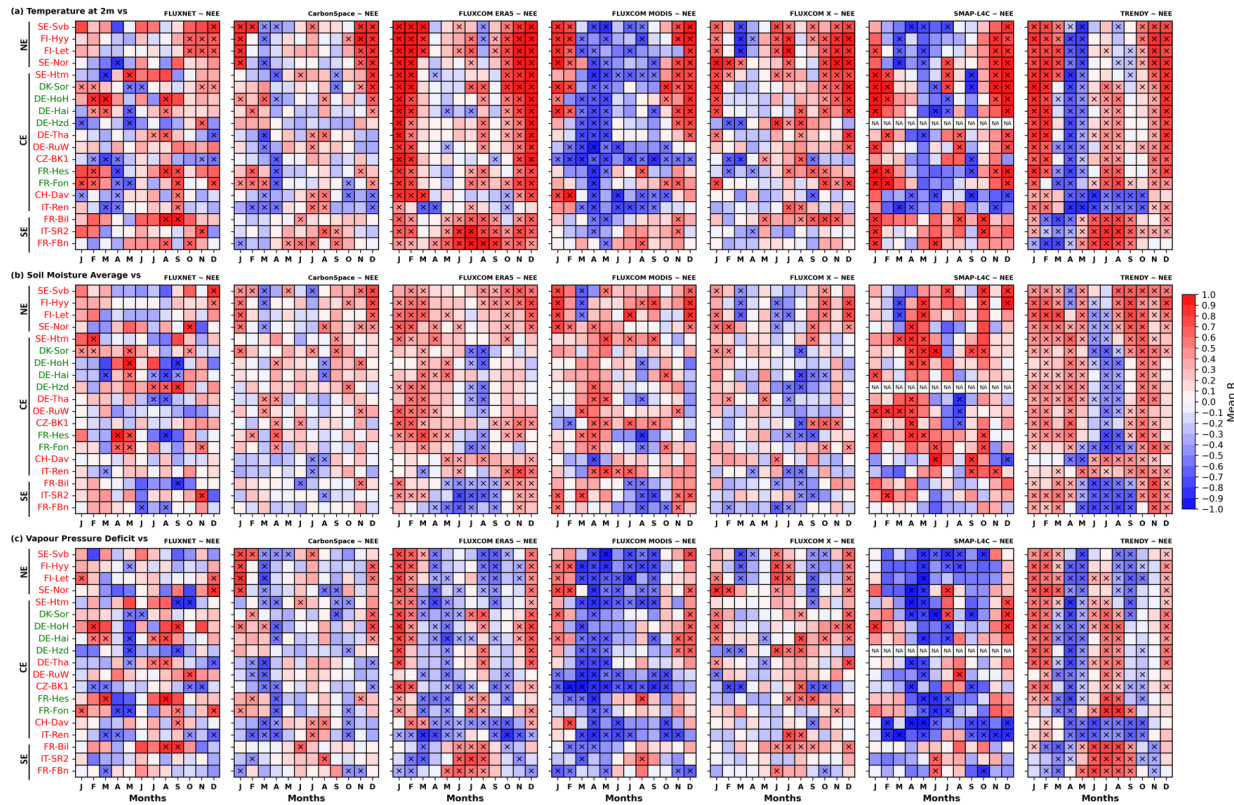


Figure 9. Same as Fig. 8 but using monthly anomalies calculated after removing the mean annual cycle.

a supprimé:

... The NEE-SM<sub>AVG</sub> relationship, however, varies between northern and central Europe. In northern Europe, depending on the dataset, SM<sub>AVG</sub> and NEE interannual variability are not consistently linked, with correlations either weak and insignificant or strong but inconsistent throughout the spring season (Fig. 9b). In contrast, a clear relationship emerges in central Europe, where correlations are significantly positive across most sites and datasets, though their strength remains uncertain (with SMAP-L4C showing much larger correlation values). The increase in spring CO<sub>2</sub> sequestration under anomalously dry soil conditions is likely driven by elevated T<sub>2m</sub> and VPD, leading to enhanced evapotranspiration and drier soils. During the peak of the summer season (July–August), NEE is positively correlated with T<sub>2m</sub> and VPD and negatively correlated with soil moisture across most sites in northern and central Europe.



**Figure 10.** Interannual co-variability between NEE and (a) 2 m temperature, (b) soil moisture and (c) vapour pressure deficit for each month, all sites and all datasets. The co-variability is assessed through Bravais Pearson correlation computed for each month between CO<sub>2</sub> fluxes and ERA5-Land climate data. The number of years included varies depending on the data, as shown in Fig. 2d. Correlation values marked with 'x' are significant at the 95% confidence level according to the Bravais-Pearson test. Cells labelled 'NA' indicate cases where CO<sub>2</sub> flux data are corrupted (SMAP-LAC). For conciseness, correlations are computed using the ensemble mean of CO<sub>2</sub> fluxes for FLUXCOM (ERA5 and MODIS) and TRENDY models. ENF sites are displayed in red text, while DBF sites are highlighted in green. Sites are ordered from north to south based on their latitude, with black vertical lines indicating the boundaries between northern (NE), central (CE) and southern (SE) Europe.

a supprimé: 9

#### 4 Discussion

This study aims at assessing the impact of climate on annual cycle and interannual variability of monthly CO<sub>2</sub> fluxes in European DBFs and ENFs through conjointly analysing observations from the FLUXNET network and state-of-the-art data-driven and process-based models.

As a first step, we assess the model abilities to reproduce the observed mean annual cycle and interannual variability of CO<sub>2</sub> fluxes. This evaluation presents two key challenges. First, the temporal coverage of observations in the FLUXNET database is often limited, making it difficult to extract robust signals, particularly for interannual variability. Site-specific characteristics may also cause a disconnect between CO<sub>2</sub> flux variability and regional climate variability (Chu et al., 2017). Second, there is a spatial scale mismatch between site-level observations, representing fluxes from the tower footprint to several square kilometers (Göckede et al., 2008), and most models used in this study, which simulate fluxes at regional to large scales, except for the hectometric-scale CarbonSpace model. Given these constraints, our evaluation should be considered qualitative rather than strictly quantitative.

The models reasonably capture both the annual cycle and interannual variability of observed CO<sub>2</sub> fluxes, though with some magnitude discrepancies. In particular, the models accurately capture the north-to-south gradient, with increased length in the CO<sub>2</sub> sequestration period from northern to southern Europe, as well as the more pronounced annual cycle in DBFs than ENFs. With the exception of the CarbonSpace model, which overestimates CO<sub>2</sub> sequestration across all European sites, most models tend to underestimate GPP and overestimate RECO, resulting in a near systematic underestimation of CO<sub>2</sub> sequestration.

The interannual variability in the models is weaker than in the observations, consistent with previous studies (e.g., Nelson et al., 2024). However, the CarbonSpace data-driven model proved to be the only model tested that does not underestimate the NEE interannual variability. The reasons may involve its high spatial resolution (few hectares) and the use of a Lagrangian particle dispersion model, which allows it to closely align with the flux tower footprints. This results in more precise flux localization, which may improve its response to fine-scale variability. They may also involve the use of an ensemble tree method for regression. This method offers greater flexibility in capturing nonlinear interactions between environmental variables and NEE. Further studies are needed to evaluate these hypotheses. The temporal co-variability between observed and simulated CO<sub>2</sub> fluxes remains correct despite the underestimated magnitude in CO<sub>2</sub> flux interannual variability. This agreement was expected for data-driven models, as they incorporate FLUXNET observations in their development. However, it was less anticipated for process-based models, which do not assimilate direct CO<sub>2</sub> flux measurements. Their ability to capture observed interannual variability likely stems from the fact that TRENDY models are driven by observed CO<sub>2</sub> concentrations, land-use changes, and climate data, while the SMAP-L4C model benefits from the assimilation of satellite-derived soil moisture observations.

Despite uncertainties, our results highlight that state-of-the-art models are valuable tools for complementing observations, particularly in assessing the impact of climate on the interannual variability of CO<sub>2</sub> fluxes at the

**a supprimé:** In southern Europe (FR-Bil, IT-SR2, and FR-FBn), the influence of climate on NEE interannual variability is more uncertain, particularly for T<sub>2m</sub> and VPD, as both the sign and strength of their correlations with NEE vary across datasets. Correlations are generally weak and/or barely significant in the observations, the CarbonSpace model, FLUXCOM-MODIS, and SMAP-L4C models. In FLUXCOM-ERA5, the correlation signs for T<sub>2m</sub> and VPD are inconsistent (except in summer), whereas in TRENDY, they remain consistent except in fall. This inconsistency is not observed for GPP and RECO (Figs. A6–7). In summer, most datasets indicate that anomalously low T<sub>2m</sub> and VPD, along with anomalously high S<sub>MAP</sub>, enhance both GPP and RECO. This suggests that NEE interannual variability in southern Europe results from a complex interplay between GPP and RECO contributions. Moreover, the opposing correlation signs between NEE–T<sub>2m</sub> and NEE–VPD in southern Europe suggest that VPD in drier, hotter environments is more strongly influenced by atmosphere-surface feedbacks than by large-scale atmospheric conditions. In contrast, the impact of S<sub>MAP</sub> on NEE interannual variability shows greater inter-dataset agreement (Fig. 9b), with positive correlations in winter and fall and negative correlations in summer. This indicates that excess winter precipitation, leading to wetter soils, enhances CO<sub>2</sub> release, whereas increased summer precipitation or reduced evapotranspiration promotes CO<sub>2</sub> sequestration.¶

**a supprimé:** Yet, t

**a supprimé:** the aforementioned constraints

**a mis en forme :** Indice

**a supprimé:** ,

European scale. The relationship between CO<sub>2</sub> fluxes and climate is analysed for both the annual cycle and interannual variability using synchronous correlation analyses between each CO<sub>2</sub> flux and individual climate variables, including 2 m temperature (T<sub>2m</sub>), vapour pressure deficit (VPD), and soil moisture (SM<sub>AVG</sub>).

Regarding the annual cycle, the influence of climate on CO<sub>2</sub> fluxes is stronger in northern and central Europe than in southern Europe, where seasonal climate variations are less pronounced. In southern Europe, both the agreement between observations and models and the consistency among different data-driven and process-based models are weaker. The spread within members (FLUXCOM-ERA5 and FLUXCOM-MODIS), and DVGMs (TRENDY), is also larger. We hypothesize that part of this model uncertainty stems from the limited number of ENF sites in southern Europe, leading to weak constraints for data-driven models and fewer reference points for calibrating DVGMs. However, it is worth noting that the uncertainty associated with the machine learning methods used to develop data-driven models remains low, whereas inter-DGVM spread can be substantial.

Regarding interannual variability, the climate impact on CO<sub>2</sub> fluxes can be summarized in three points. First, climate impacts more strongly GPP and RECO than NEE, regardless of the site and dataset. Since NEE is the difference between GPP and RECO, its interannual variability arises from various combinations of these two components. For instance, reduced CO<sub>2</sub> sequestration can result from a greater increase in RECO compared to GPP, a larger decrease in GPP than in RECO, a decrease in GPP with no change in RECO, or an increase in RECO without any change in GPP. Such complexity implies that the influence of climate on NEE is less direct and likely more intricate than its effects on GPP and RECO. Second, the impact of climate on interannual variability of CO<sub>2</sub> fluxes depends strongly on how it is assessed. It appears weak when monthly anomalies from all months are analyzed together but becomes more pronounced when each month is examined separately, revealing seasonal shifts in the sign of the climate-NEE relationship. The timing and direction of these seasonal shifts vary across datasets and regions. In particular, CO<sub>2</sub> sequestration is enhanced by anomalously low T<sub>2m</sub> and VPD and anomalously high SM<sub>AVG</sub> in summer, whereas the opposite pattern prevails in spring. This finding aligns with previous case studies showing that heatwaves and droughts reduce summer CO<sub>2</sub> sequestration (Ciais et al., 2005; Smith et al., 2020; Thompson et al., 2020; van der Woude et al., 2023). It also highlights that anomalously warm and dry springs may, in some cases, enhance CO<sub>2</sub> sequestration, likely because soil moisture levels remain sufficient during this period, in line with e.g. Delpierre et al. (2009) and Smith et al. (2020). Such a transition from spring to summer is less evident in southern Europe, which instead exhibits consistent patterns from spring to summer. The climate-NEE relationship is much noisier in both space and time in the observations than in the models, and it can vary substantially across different models. This indicates that local flux measurements may not reliably represent regional-scale dynamics, while models may exaggerate the influence of climate on CO<sub>2</sub> flux variability (despite underestimating its magnitude). Further work is needed to disentangle site-specific effects from broader-scale signals, a critical step toward improving the calibration of regional and global models that cannot resolve local heterogeneity.

## 5. Conclusion

**a supprimé:** by significantly expanding the number of studied years and the spatial domain

**a supprimé:** s

**a supprimé:** Second,

**a supprimé:** In northern and central Europe, most models indicate that

**a supprimé:** contrasting patterns between late fall–winter and early spring–early fall

**a supprimé:** ¶ the climate impact significantly changes along the annual cycle with noticeable differences between northern/central and southern Europe, regardless of land cover class. For conciseness, we discuss only results for NEE. In northern and central Europe, CO<sub>2</sub> sequestration is closely linked to T<sub>2m</sub> and VPD, whereas in southern Europe, soil moisture emerges as the dominant driver. These findings reinforce the role of soil moisture as the primary control on NEE in southern Europe, though not necessarily on its components (i.e., GPP and RECO), refining previous studies (Seddon et al., 2016; Madani et al., 2017). ¶

¶ Finally, we acknowledge that the general patterns discussed above do not always hold at specific sites. This suggests the influence of additional factors, such as soil properties, forest management practices, tree age and tree species (see references in the Introduction). Assessing the impact of these factors on CO<sub>2</sub> flux variability falls beyond the scope of this study, as it would require detailed site-specific information not available in the FLUXNET database and not fully represented in the models used. ¶

852 This study makes use of state-of-the-art data-driven and process-based models to complement observations for  
853 assessing the impact of climate on the annual cycle and interannual variability of monthly CO<sub>2</sub> fluxes in European  
854 DBFs and ENFs. Output from different data-driven models (CarbonSpace and FLUXCOM-ERA5, -MODIS and  
855 -X) and process-based models forced by realistic conditions (assimilation of satellite derived soil moisture in  
856 SMAP-L4C and time-varying CO<sub>2</sub> concentration, land-use and climate in TRENDY DVGMs) are analysed  
857 conjointly with CO<sub>2</sub> measurements from 19 sites (6 DBFs and 13 ENFs) of the FLUXNET network. Across  
858 Europe, a clear north-south gradient emerges in the annual cycle of CO<sub>2</sub> fluxes. The length of the CO<sub>2</sub> sequestration  
859 season increases southwards in link with more favourable climate conditions for photosynthesis in southern than  
860 northern Europe. This large-scale pattern is perturbed locally by site elevation and other site factors not included  
861 in the study (e.g., soil properties and forest age). It is also perturbed by land cover class, with more pronounced  
862 annual cycle of DBFs than ENFs in central Europe. The interannual variability of CO<sub>2</sub> fluxes does not exhibit such  
863 a north-south gradient, regardless of the metric used (standard deviation or coefficient of variation). However, it  
864 remains strong across all seasons, with spring and summer showing high variability based on standard deviation,  
865 and autumn and winter based on the coefficient of variation.  
866  
867 The models accurately capture the observed features despite magnitude differences. Compared to observations,  
868 the CO<sub>2</sub> sequestration is weaker in regional-scale models and stronger in the hectometric-scale CarbonSpace data-  
869 driven model. Except the CarbonSpace model, all models systematically underestimate the interannual variability  
870 of CO<sub>2</sub> fluxes, as already reported (Lin et al. 2023; Nelson et al., 2024). Despite biased magnitude, the interannual  
871 variability of modelled fluxes correlates well with the observations. This supports the use of models to complement  
872 observations, whose limited temporal coverage and site specificities hinders the assessment of climate impacts on  
873 CO<sub>2</sub> interannual variability. We show that the influence of climate on CO<sub>2</sub> flux interannual variability is obscured  
874 when monthly anomalies are analyzed together. This apparent lack of relationship masks distinct seasonal patterns,  
875 which are concealed when considering all months together. Winter and fall CO<sub>2</sub> release increases under elevated  
876 temperature and VPD in northern and central Europe, while no clear signal emerges in southern Europe. The CO<sub>2</sub>  
877 sequestration increases under anomalously hot and dry conditions in spring and cold and wet conditions in summer  
878 in northern/central Europe. Anomalously cold and wet conditions also favor CO<sub>2</sub> sequestration in southern Europe  
879 from spring to summer. While these seasonal signals appear noisy in the observations, due to limited sample sizes  
880 and site-specific variability, they emerge more clearly in the models, albeit with some model-dependent  
881 differences.  
882  
883 These results highlight the significant space-time variability in the impact of climate on forest CO<sub>2</sub> fluxes across  
884 Europe. This variability underscores the importance of considering regional and seasonal differences when  
885 assessing the effects of climate change on CO<sub>2</sub> fluxes. Neglecting these variations could lead to oversimplified  
886 conclusions and hinder the development of accurate predictions and effective mitigation strategies.  
887

a supprimé: All

a supprimé: However

a supprimé: The

a supprimé: changes along the annual cycle and a clear distinction emerges between northern/central Europe and southern Europe despite model dependencies. Atmospheric factors (i.e., 2 m temperature and vapour pressure deficit) dominate CO<sub>2</sub> fluxes interannual variability in northern and central Europe, while soil moisture dominates in southern Europe. ...

a supprimé: and under low VPD

a supprimé: from

a supprimé: May to September

901 Appendices

902

903

904

**Table A1.** List of TRENDY DVGMS used in this study.

DVGM	Reference
CABLE-POP	Haverd et al. (2018)
CLM5.0	Lawrence et al. (2019)
DLEM	Tian et al. (2016)
JULES	Best et al. (2011); Clark et al. (2011)
LPX-Bern	Lienert and Joos (2018)
OCN	Zachle et al. (2010)
ORCHIDEE	Krinner et al. (2005)
SDGVM	Woodward and Lomas (2004)
ISBA-CTRIP	Delire et al. (2020)
IBIS	Xia et al. (2015); Jinxun et al. (2022)
CLASSIC	Seiler et al. (2021)
EDv3	Longo et al. (2019)
E3SM	Golaz et al. (2019)
LPJmL	Bondeau et al. (2007)
LPJwsl	Gerten et al. (2004)

*Columns 1 and 2 provide the name of the DGVM and its corresponding reference, respectively.*

905

906

907  
908

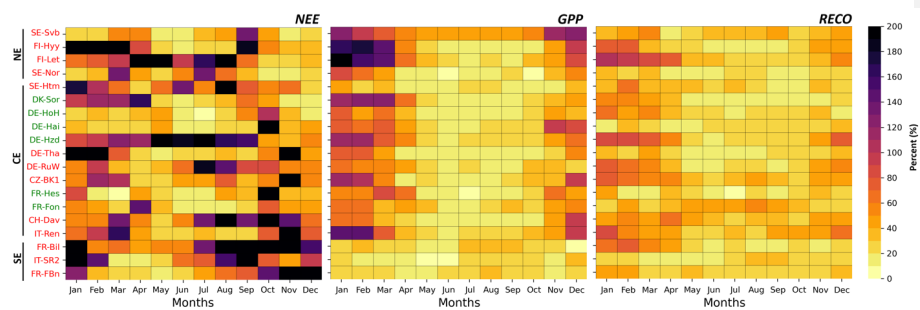


**Figure A1.** Same as Fig. 4b but using the coefficient of variation as a metric for interannual variability.



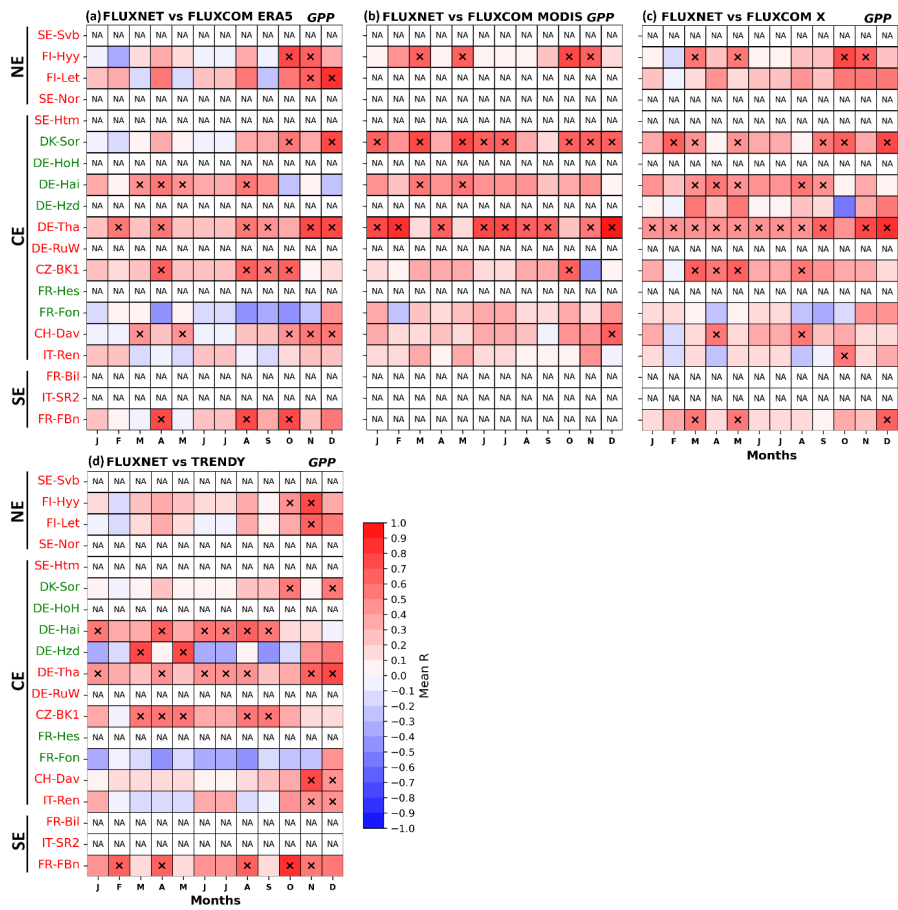


Figure A2. Same as Fig. 7 but for GPP.

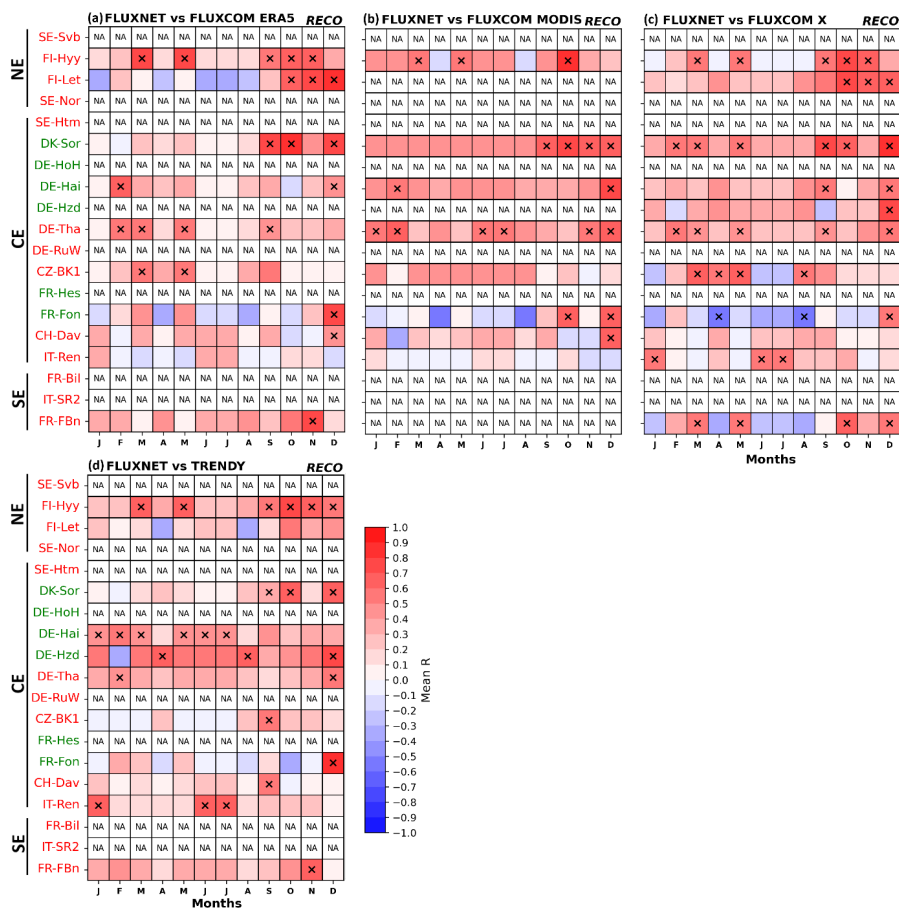
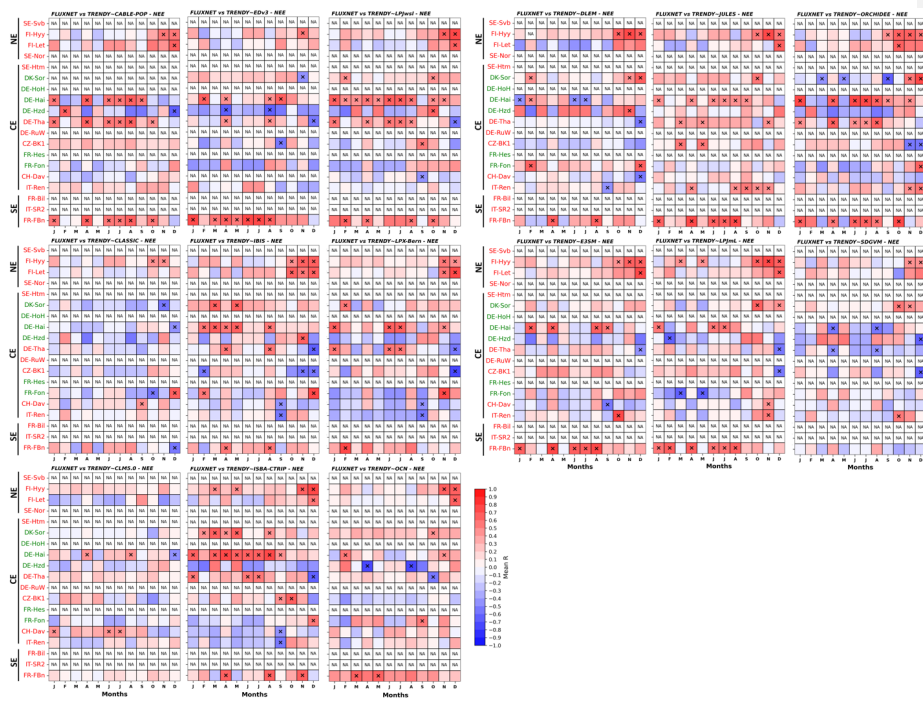
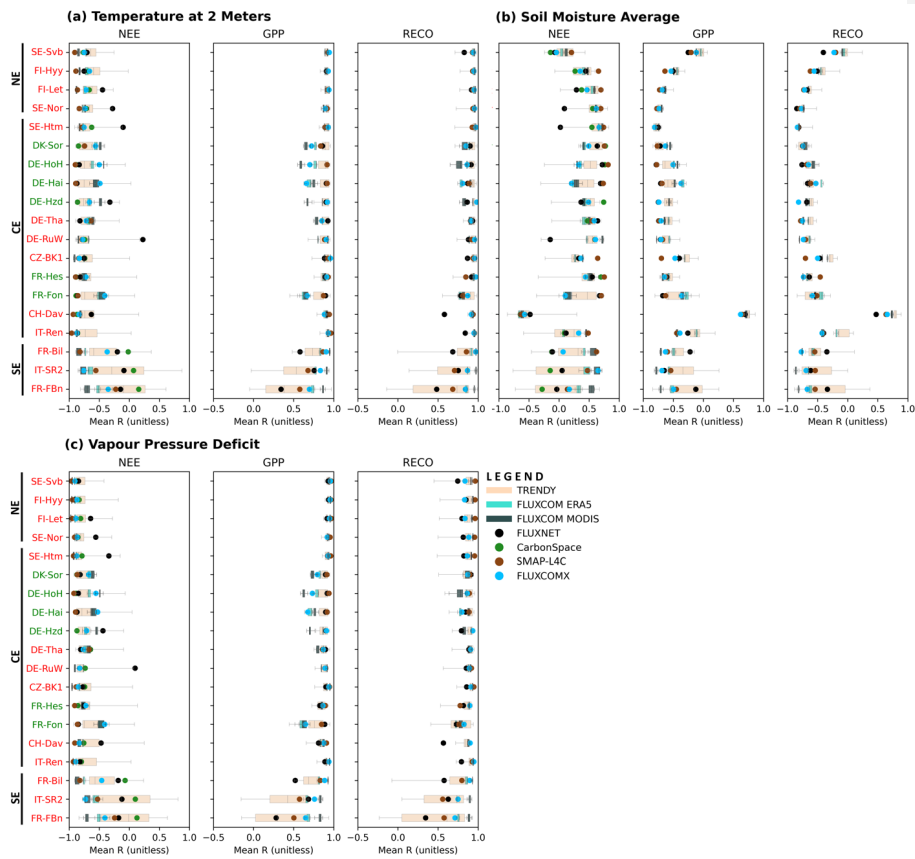


Figure A3. Same as Fig. 7 but for RECO.

913  
914

**Figure A4.** Same as Fig. 7e but for each TRENDY model considered in this study.





**Figure A5.** Same as Fig. 5 but for the relationship between the annual cycle of CO<sub>2</sub> fluxes and (a) 2 m temperature, (b) soil moisture, and (c) vapour pressure deficit. This relationship is evaluated using Bravais-Pearson correlation. For details, refer to the legend caption of Fig. 8.

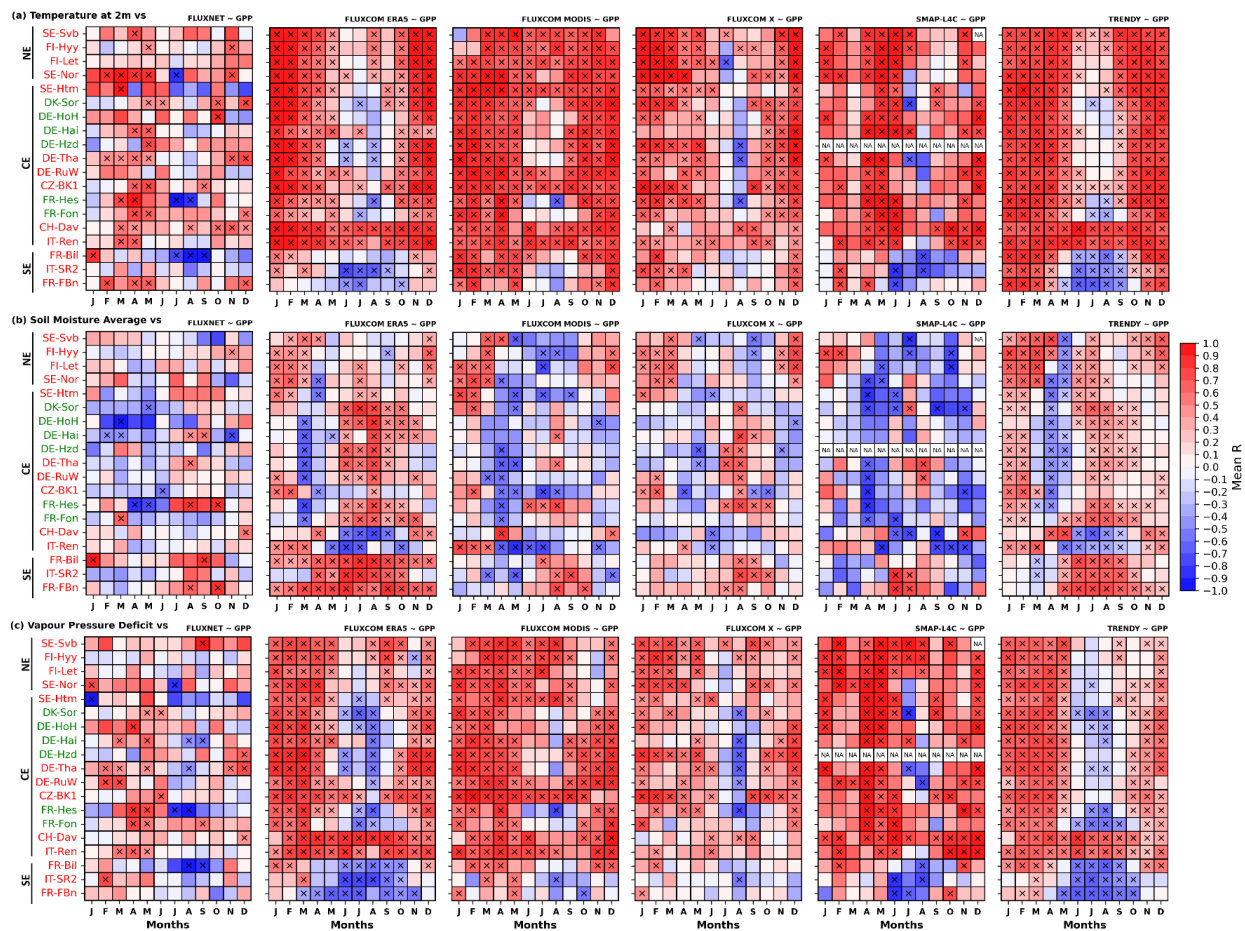


Figure A6. Same as Fig. 10 but for GPP.

a supprimé: 9

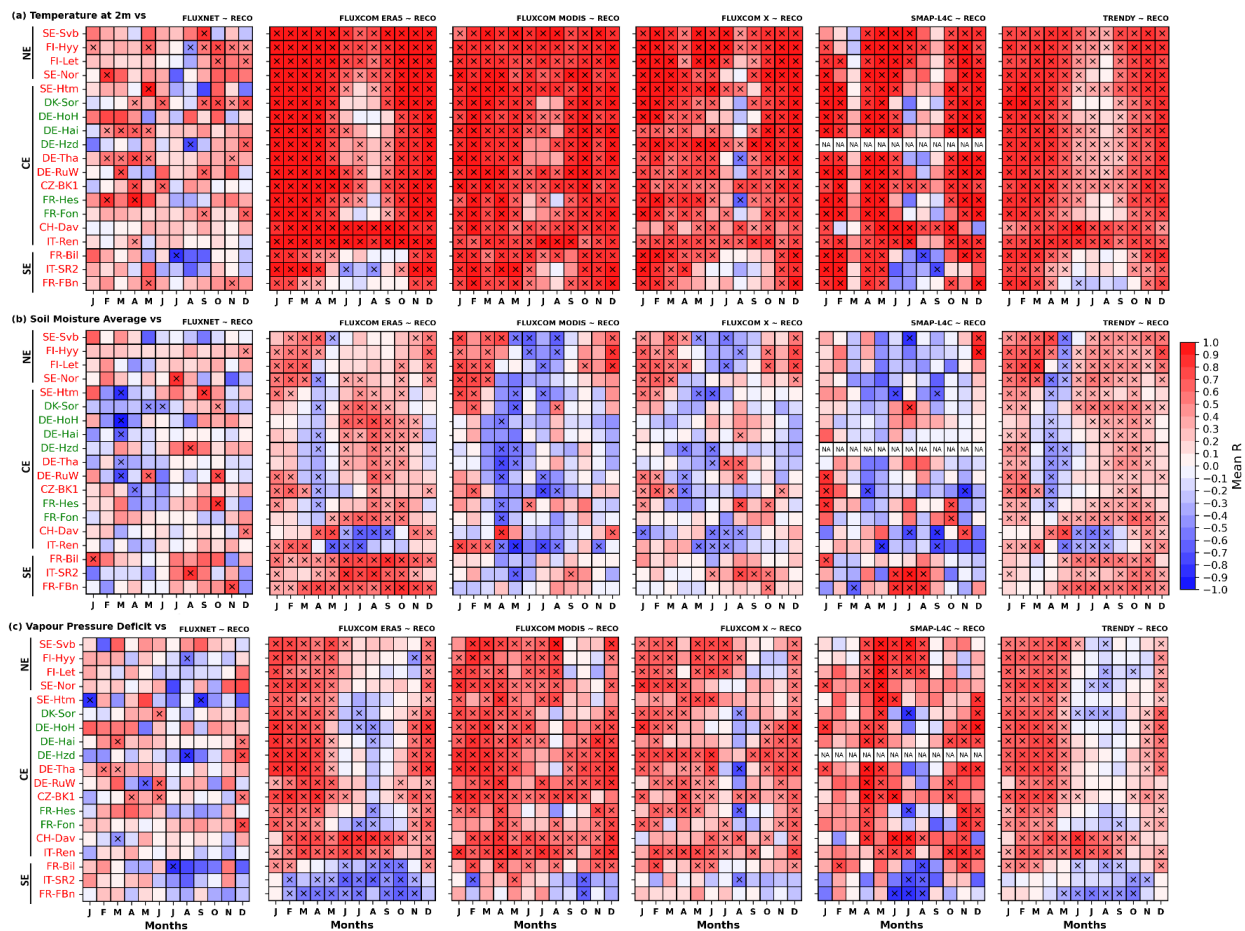


Figure A7. Same as Fig. 10 but for GPP.

a supprimé: 9

925 **Author contribution**

926  
927 JC conceived the study. JC, AU, and GM collected the data and developed the analysis scripts. GM and JC drafted  
928 the first version of the manuscript. AU and JC drafted the second version. All co-authors contributed to its review.  
929

931 **Acknowledgement**

932  
933 This work is funded by the French National Research Agency (ANR-22-CPJ2-0026-01) and is part of the  
934 "Laboratoire d'expérimentation forestière du mont Beuvray", supported by the European Union (EAFRD) and the  
935 Région Bourgogne-Franche-Comté, as part of the agricultural European Innovation Partnership (EIP-AGRI). We  
936 thank Daniel Berveiller for useful discussions on eddy covariance measurements and the ~~three~~ anonymous  
937 reviewers for constructive comments.  
938  
939

940 **Data Availability**

941  
942 Climate parameters from the ERA5-Land are available at [https://cds.climate.copernicus.eu/datasets/reanalysis-](https://cds.climate.copernicus.eu/datasets/reanalysis-era5-land)  
943 [era5-land](https://cds.climate.copernicus.eu/datasets/reanalysis-era5-land). CO<sub>2</sub> fluxes from the FLUXOM data-driven model are available at <https://www.bgc-jena.mpg.de> and  
944 [https://meta.icos-cp.eu/collections/zfwf1Ak2I7OlziGDTX8XI6\\_T](https://meta.icos-cp.eu/collections/zfwf1Ak2I7OlziGDTX8XI6_T). Those from TRENDY and SMAP-L4C  
945 process-based models are available on request to Professor Stephan Sitch ([s.a.sitch@exeter.ac.uk](mailto:s.a.sitch@exeter.ac.uk)) and at  
946 <https://nsidc.org/data/spl4cmdl/versions/7>, respectively.

949 **Conflict of Interest**

950  
951 The authors declare no competing interests.  
952  
953

954 **References**

955  
956 Besnard, S., Carvalhais, N., Arain, M. A., Black, A., De Bruin, S., Buchmann, N., Cescatti, A., Chen, J., Clevers,  
957 J. G. P. W., Desai, A. R., Gough, C. M., Havrankova, K., Herold, M., Hörtnagl, L., Jung, M., Knohl, A.,  
958 Kruijt, B., Krupkova, L., Law, B. E., Lindroth, A., Noormets, A., Roupsard, O., Steinbrecher, R., Varlagin,  
959 A., Vincke, C., and Reichstein, M.: Quantifying the effect of forest age in annual net forest carbon balance,

a supprimé: two

Code de champ modifié

Code de champ modifié

Code de champ modifié

Code de champ modifié

Code de champ modifié

- Environ. Res. Lett., 13, <https://doi.org/10.1088/1748-9326/AAEAEB>, 2018.
- Best, M. J., Pryor, M., Clark, D. B., Rooney, G. G., Essery, R. L. H., Ménard, C. B., Edwards, J. M., Hendry, M. A., Porson, A., Gedney, N., Mercado, L. M., Sitch, S., Blyth, E., Boucher, O., Cox, P. M., Grimmond, C. S. B., and Harding, R. J.: The Joint UK Land Environment Simulator (JULES), model description – Part 1: Energy and water fluxes, *Geosci. Model Dev.*, 4, 677–699, <https://doi.org/10.5194/GMD-4-677-2011>, 2011.
- Bondeau, A., Smith, P. C., Zaehle, S., Schaphoff, S., Lucht, W., Cramer, W., Gerten, D., Lotze-campen, H., Müller, C., Reichstein, M., and Smith, B.: Modelling the role of agriculture for the 20th century global terrestrial carbon balance, *Glob. Chang. Biol.*, 13, 679–706, <https://doi.org/10.1111/J.1365-2486.2006.01305.X>, 2007.
- Burba, G.: Atmospheric flux measurements, *Adv. Spectrosc. Monit. Atmos.*, 443–520, <https://doi.org/10.1016/B978-0-12-815014-6.00004-X>, 2021.
- Cai, W. and Prentice, I. C.: Recent trends in gross primary production and their drivers: analysis and modelling at flux-site and global scales, *Environ. Res. Lett.*, 15, 124050, <https://doi.org/10.1088/1748-9326/ABC64E>, 2020.
- Carrara, A., Kowalski, A. S., Neirynck, J., Janssens, I. A., Yuste, J. C., and Ceulemans, R.: Net ecosystem CO<sub>2</sub> exchange of mixed forest in Belgium over 5 years, *Agric. For. Meteorol.*, 119, 209–227, [https://doi.org/10.1016/S0168-1923\(03\)00120-5](https://doi.org/10.1016/S0168-1923(03)00120-5), 2003.
- Carrara, A., Janssens, I. A., Curiel Yuste, J., and Ceulemans, R.: Seasonal changes in photosynthesis, respiration and NEE of a mixed temperate forest, *Agric. For. Meteorol.*, 126, 15–31, <https://doi.org/10.1016/J.AGRFORMET.2004.05.002>, 2004.
- Chen, T., and Guestrin C.: Xgboost: A scalable tree boosting system. In Proceedings of the 22nd ACM SIGKDD international conference on knowledge discovery and data mining, 785–794. <https://doi.org/10.1145/2939672.2939785>, 2016.
- Chu, H., Baldocchi, D. D., John, R., Wolf, S., and Reichstein, M.: Fluxes all of the time? A primer on the temporal representativeness of FLUXNET, *JGR Biogeosciences*, 122, 289–307, <https://doi.org/10.1002/2016JG003576>, 2017.
- Ciais, P., Reichstein, M., Viovy, N., Granier, A., Ogée, J., Allard, V., Aubinet, M., Buchmann, N., Bernhofer, C., Carrara, A., Chevallier, F., De Noblet, N., Friend, A. D., Friedlingstein, P., Grünwald, T., Heinesch, B., Keronen, P., Knohl, A., Krinner, G., Loustau, D., Manca, G., Matteucci, G., Miglietta, F., Ourcival, J. M., Papale, D., Pilegaard, K., Rambal, S., Seufert, G., Soussana, J. F., Sanz, M. J., Schulze, E. D., Vesala, T., and Valentini, R.: Europe-wide reduction in primary productivity caused by the heat and drought in 2003, *Nat.* 2005 4377058, 437, 529–533, <https://doi.org/10.1038/nature03972>, 2005.
- Clark, D. B., Mercado, L. M., Sitch, S., Jones, C. D., Gedney, N., Best, M. J., Pryor, M., Rooney, G. G., Essery, R. L. H., Blyth, E., Boucher, O., Harding, R. J., Huntingford, C., and Cox, P. M.: The Joint UK Land Environment Simulator (JULES), model description – Part 2: Carbon fluxes and vegetation dynamics, *Geosci. Model Dev.*, 4, 701–722, <https://doi.org/10.5194/GMD-4-701-2011>, 2011.
- Curtis, P. S. and Gough, C. M.: Forest aging, disturbance and the carbon cycle, *New Phytol.*, 219, 1188–1193, <https://doi.org/10.1111/NPH.15227>, 2018.
- Delire, C., Séférian, R., Decharme, B., Alkama, R., Calvet, J. C., Carrer, D., Gibelin, A. L., Joetzjer, E., Morel, X., Rocher, M., and Tzanos, D.: The Global Land Carbon Cycle Simulated With ISBA-CTRIP: Improvements Over the Last Decade, *J. Adv. Model. Earth Syst.*, 12, e2019MS001886, <https://doi.org/10.1029/2019MS001886>, 2020.
- Delpierre, N., Soudani, K., François, C., Köstner, B., Pontailier, J. Y., Nikinmaa, E., Misson, L., Aubinet, M., Bernhofer, C., Granier, A., Grünwald, T., Heinesch, B., Longdoz, B., Ourcival, J. M., Rambal, S., Vesala, T., and Dufrêne, E.: Exceptional carbon uptake in European forests during the warm spring of 2007: a data–model analysis, *Glob. Chang. Biol.*, 15, 1455–1474, <https://doi.org/10.1111/J.1365-2486.2008.01835.X>, 2009.
- Endsley, K. A., Kimball, J. S., Kundig, T., Reichle, R. H., and Ardizzone, J. V: Validation Assessment for the Soil Moisture Active Passive (SMAP) Level 4 Carbon (L4\_C) Data Product Version 7, 2023.

Code de champ modifié



- Friedlingstein, P., Cox, P., Betts, R., Bopp, L., von Bloh, W., Brovkin, V., Cadule, P., Doney, S., Eby, M., Fung, I., Bala, G., John, J., Jones, C., Joos, F., Kato, T., Kawamiya, M., Knorr, W., Lindsay, K., Matthews, H. D., Raddatz, T., Rayner, P., Reick, C., Roeckner, E., Schnitzler, K. G., Schnur, R., Strassmann, K., Weaver, A. J., Yoshikawa, C., and Zeng, N.: Climate–Carbon Cycle Feedback Analysis: Results from the C4MIP Model Intercomparison, *J. Clim.*, 19, 3337–3353, <https://doi.org/10.1175/JCLI3800.1>, 2006.
- Friedlingstein, P., O’Sullivan, M., Jones, M. W., Andrew, R. M., Bakker, D. C. E., Hauck, J., Landschützer, P., Le Quéré, C., Luijkx, I. T., Peters, G. P., Peters, W., Pongratz, J., Schwingshackl, C., Sitch, S., Canadell, J. G., Ciais, P., Jackson, R. B., Alin, S. R., Anthoni, P., Barbero, L., Bates, N. R., Becker, M., Bellouin, N., Decharme, B., Bopp, L., Brasika, I. B. M., Cadule, P., Chamberlain, M. A., Chandra, N., Chau, T. T. T., Chevallier, F., Chini, L. P., Cronin, M., Dou, X., Enyo, K., Evans, W., Falk, S., Feely, R. A., Feng, L., Ford, D. J., Gasser, T., Ghattas, J., Gkritzalis, T., Grassi, G., Gregor, L., Gruber, N., Gürses, Ö., Harris, I., Hefner, M., Heinke, J., Houghton, R. A., Hurtt, G. C., Iida, Y., Ilyina, T., Jacobson, A. R., Jain, A., Jarníková, T., Järsild, A., Jiang, F., Jin, Z., Joos, F., Kato, E., Keeling, R. F., Kennedy, D., Goldewijk, K. K., Knauer, J., Korsbakken, J. I., Körtzinger, A., Lan, X., Lefèvre, N., Li, H., Liu, J., Liu, Z., Ma, L., Marland, G., Mayot, N., McGuire, P. C., McKinley, G. A., Meyer, G., Morgan, E. J., Munro, D. R., Nakaoka, S. I., Niwa, Y., O’Brien, K. M., Olsen, A., Omar, A. M., Ono, T., Paulsen, M., Pierrot, D., Pocock, K., Poulter, B., Powis, C. M., Rehder, G., Resplandy, L., Robertson, E., Rödenbeck, C., Rosan, T. M., Schwinger, J., Séférian, R., et al.: Global Carbon Budget 2023, *Earth Syst. Sci. Data*, 15, 5301–5369, <https://doi.org/10.5194/ESSD-15-5301-2023>, 2023.
- Gerten, D., Schaphoff, S., Haberlandt, U., Lucht, W., and Sitch, S.: Terrestrial vegetation and water balance—hydrological evaluation of a dynamic global vegetation model, *J. Hydrol.*, 286, 249–270, <https://doi.org/10.1016/J.JHYDROL.2003.09.029>, 2004.
- Göckede, M., Foken, T., Aubinet, M., Aurela, M., Banza, J., Bernhofer, C., Bonnefond, J. M., Brunet, Y., Carrara, A., Clement, R., Dellwik, E., Elbers, J., Eugster, W., Fuhrer, J., Granier, A., Grünwald, T., Heinesch, B., Janssens, I. A., Knohl, A., Koeble, R., Laurila, T., Longdoz, B., Manca, G., Marek, M., Markkanen, T., Mateus, J., Matteucci, G., Mauder, M., Migliavacca, M., Minerbi, S., Moncrieff, J., Montagnani, L., Moors, E., Ourcival, J. M., Papale, D., Pereira, J., Pilegaard, K., Pita, G., Rambal, S., Rebmann, C., Rodrigues, A., Rotenberg, E., Sanz, M. J., Sedlak, P., Seufert, G., Siebicke, L., Soussana, J. F., Valentini, R., Vesala, T., Verbeeck, H., and Yakir, D.: Quality control of CarboEurope flux data - Part 1: Coupling footprint analyses with flux data quality assessment to evaluate sites in forest ecosystems, *Biogeosciences*, 5, 433–450, <https://doi.org/10.5194/BG-5-433-2008>, 2008.
- Golaz, J. C., Caldwell, P. M., Van Roekel, L. P., Petersen, M. R., Tang, Q., Wolfe, J. D., Abeshu, G., Anantharaj, V., Asay-Davis, X. S., Bader, D. C., Baldwin, S. A., Bisht, G., Bogenschutz, P. A., Branstetter, M., Brunke, M. A., Brus, S. R., Burrows, S. M., Cameron-Smith, P. J., Donahue, A. S., Deakin, M., Easter, R. C., Evans, K. J., Feng, Y., Flanner, M., Foucar, J. G., Fyke, J. G., Griffin, B. M., Hannay, C., Harrop, B. E., Hoffman, M. J., Hunke, E. C., Jacob, R. L., Jacobsen, D. W., Jeffery, N., Jones, P. W., Keen, N. D., Klein, S. A., Larson, V. E., Leung, L. R., Li, H. Y., Lin, W., Lipscomb, W. H., Ma, P. L., Mahajan, S., Maltrud, M. E., Mamatjanov, A., McClean, J. L., McCoy, R. B., Neale, R. B., Price, S. F., Qian, Y., Rasch, P. J., Reeves Eyre, J. E. J., Riley, W. J., Ringler, T. D., Roberts, A. F., Roesler, E. L., Salinger, A. G., Shaheen, Z., Shi, X., Singh, B., Tang, J., Taylor, M. A., Thornton, P. E., Turner, A. K., Veneziani, M., Wan, H., Wang, H., Wang, S., Williams, D. N., Wolfram, P. J., Worley, P. H., Xie, S., Yang, Y., Yoon, J. H., Zelinka, M. D., Zender, C. S., Zeng, X., Zhang, C., Zhang, K., Zhang, Y., Zheng, X., Zhou, T., and Zhu, Q.: The DOE E3SM Coupled Model Version 1: Overview and Evaluation at Standard Resolution, *J. Adv. Model. Earth Syst.*, 11, 2089–2129, <https://doi.org/10.1029/2018MS001603>, 2019.
- Hardouin, L., Delire, C., Decharme, B., Lawrence, D. M., Nabel, J. E. M. S., Brovkin, V., Collier, N., Fisher, R., Hoffman, F. M., Koven, C. D., Séférian, R., and Stacke, T.: Uncertainty in land carbon budget simulated by terrestrial biosphere models: the role of atmospheric forcing, *Environ. Res. Lett.*, 17, 094033, <https://doi.org/10.1088/1748-9326/AC888D>, 2022.
- Haszpra, L., Barcza, Z., Davis, K. J., and Tarczay, K.: Long-term tall tower carbon dioxide flux monitoring over an area of mixed vegetation, *Agric. For. Meteorol.*, 132, 58–77, <https://doi.org/10.1016/J.AGRFORMET.2005.07.002>, 2005.
- Haverd, V., Smith, B., Nieradzik, L., Briggs, P. R., Woodgate, W., Trudinger, C. M., Canadell, J. G., and Cuntz,

- M.: A new version of the CABLE land surface model (Subversion revision r4601) incorporating land use and land cover change, woody vegetation demography, and a novel optimisation-based approach to plant coordination of photosynthesis, *Geosci. Model Dev.*, 11, 2995–3026, <https://doi.org/10.5194/GMD-11-2995-2018>, 2018.
- He, B., Chen, C., Lin, S., Yuan, W., Chen, H. W., Chen, D., Zhang, Y., Guo, L., Zhao, X., Liu, X., Piao, S., Zhong, Z., Wang, R., and Tang, R.: Worldwide impacts of atmospheric vapor pressure deficit on the interannual variability of terrestrial carbon sinks, *Natl. Sci. Rev.*, 9, nwab150, <https://doi.org/10.1093/NSR/NWAB150>, 2022.
- Hersbach, H., Bell, B., Berrisford, P., Hirahara, S., Horányi, A., Muñoz-Sabater, J., Nicolas, J., Peubey, C., Radu, R., Schepers, D., Simmons, A., Soci, C., Abdalla, S., Abellan, X., Balsamo, G., Bechtold, P., Biavati, G., Bidlot, J., Bonavita, M., De Chiara, G., Dahlgren, P., Dee, D., Diamantakis, M., Dragani, R., Flemming, J., Forbes, R., Fuentes, M., Geer, A., Haimberger, L., Healy, S., Hogan, R. J., Hólm, E., Janisková, M., Keeley, S., Laloyaux, P., Lopez, P., Lupu, C., Radnoti, G., de Rosnay, P., Rozum, I., Vamborg, F., Villaume, S., and Thépaut, J. N.: The ERA5 global reanalysis, *Q. J. R. Meteorol. Soc.*, 146, 1999–2049, <https://doi.org/10.1002/QJ.3803>, 2020.
- Jinxun, L., Xuehe, L., Qian, Z., Wenping, Y., Quanzhi, Y., Zhen, Z., Qingxi, G., Carol, D., Jinxun, L., Xuehe, L., Qian, Z., Wenping, Y., Quanzhi, Y., Zhen, Z., Qingxi, G., and Carol, D.: Terrestrial Ecosystem Modeling with IBIS: Progress and Future Vision, *J. Resour. Ecol.*, 13, 2–16, <https://doi.org/10.5814/J.ISSN.1674-764X.2022.01.001>, 2022.
- Jones, L. A., Kimball, J. S., Reichle, R. H., Madani, N., Glassy, J., Ardizzone, J. V., Colliander, A., Cleverly, J., Desai, A. R., Eamus, D., Euskirchen, E. S., Hutley, L., Macfarlane, C., and Scott, R. L.: The SMAP Level 4 Carbon Product for Monitoring Ecosystem Land-Atmosphere CO<sub>2</sub> Exchange, *IEEE Trans. Geosci. Remote Sens.*, 55, 6517–6532, <https://doi.org/10.1109/TGRS.2017.2729343>, 2017.
- Jung, M., Koirala, S., Weber, U., Ichii, K., Gans, F., Camps-Valls, G., Papale, D., Schwalm, C., Tramontana, G., and Reichstein, M.: The FLUXCOM ensemble of global land-atmosphere energy fluxes, *Sci. Data* 2019 61, 6, 1–14, <https://doi.org/10.1038/s41597-019-0076-8>, 2019.
- Jung, M., Schwalm, C., Migliavacca, M., Walther, S., Camps-Valls, G., Koirala, S., Anthoni, P., Besnard, S., Bodesheim, P., Carvalhais, N., Chevallier, F., Gans, F., S Goll, D., Haverd, V., Köhler, P., Ichii, K., K Jain, A., Liu, J., Lombardozi, D., E M S Nabel, J., A Nelson, J., O’Sullivan, M., Pallandt, M., Papale, D., Peters, W., Pongratz, J., Rödenbeck, C., Sitch, S., Tramontana, G., Walker, A., Weber, U., and Reichstein, M.: Scaling carbon fluxes from eddy covariance sites to globe: Synthesis and evaluation of the FLUXCOM approach, *Biogeosciences*, 17, 1343–1365, <https://doi.org/10.5194/BG-17-1343-2020>, 2020.
- Kimball, J. S., Endsley, K. A., Jones, L. A., Kundig, T., and Reichle, R.: SMAP L4 Global Daily 9 km EASE-Grid Carbon Net Ecosystem Exchange, Version 7 | National Snow and Ice Data Center, <https://doi.org/https://doi.org/10.5067/3K9F0S1Q5J2U>, 2022.
- Kong, Z., Wang, T., Han, Q., Dai, Y., Wang, L., and Chen, X.: Evaluation of Environmental Controls on Terrestrial Net Ecosystem Exchange of CO<sub>2</sub>: A Global Perspective From the FLUXNET Sites, *J. Geophys. Res. Atmos.*, 127, e2022JD037217, <https://doi.org/10.1029/2022JD037217>, 2022.
- Krinner, G., Viovy, N., de Noblet-Ducoudré, N., Ogée, J., Polcher, J., Friedlingstein, P., Ciais, P., Sitch, S., and Prentice, I. C.: A dynamic global vegetation model for studies of the coupled atmosphere-biosphere system, *Global Biogeochem. Cycles*, 19, 1–33, <https://doi.org/10.1029/2003GB002199>, 2005.
- Kurbatova, J., Li, C., Varlagin, A., Xiao, X., and Vygodskaya, N.: Modeling carbon dynamics in two adjacent spruce forests with different soil conditions in Russia, *Biogeosciences*, 5, 969–980, <https://doi.org/10.5194/BG-5-969-2008>, 2008.
- Lasslop, G., Reichstein, M., Papale, D., Richardson, A., Arneth, A., Barr, A., Stoy, P., and Wohlfahrt, G.: Separation of net ecosystem exchange into assimilation and respiration using a light response curve approach: critical issues and global evaluation, *Glob. Chang. Biol.*, 16, 187–208, <https://doi.org/10.1111/J.1365-2486.2009.02041.X>, 2010.

- Lawrence, D. M., Fisher, R. A., Koven, C. D., Oleson, K. W., Swenson, S. C., Bonan, G., Collier, N., Ghimire, B., van Kampenhout, L., Kennedy, D., Kluzek, E., Lawrence, P. J., Li, F., Li, H., Lombardozzi, D., Riley, W. J., Sacks, W. J., Shi, M., Vertenstein, M., Wieder, W. R., Xu, C., Ali, A. A., Badger, A. M., Bisht, G., van den Broeke, M., Brunke, M. A., Burns, S. P., Buzan, J., Clark, M., Craig, A., Dahlin, K., Drewniak, B., Fisher, J. B., Flanner, M., Fox, A. M., Gentine, P., Hoffman, F., Keppel-Aleks, G., Knox, R., Kumar, S., Lenaerts, J., Leung, L. R., Lipscomb, W. H., Lu, Y., Pandey, A., Pelletier, J. D., Perket, J., Randerson, J. T., Ricciuto, D. M., Sanderson, B. M., Slater, A., Subin, Z. M., Tang, J., Thomas, R. Q., Val Martin, M., and Zeng, X.: The Community Land Model Version 5: Description of New Features, Benchmarking, and Impact of Forcing Uncertainty, *J. Adv. Model. Earth Syst.*, 11, 4245–4287, <https://doi.org/10.1029/2018MS001583>, 2019.
- Le Quéré, C., Andrew, R. M., Friedlingstein, P., Sitch, S., Pongratz, J., Manning, A. C., Korsbakken, J. I., Peters, G. P., Canadell, J. G., Jackson, R. B., Boden, T. A., Tans, P. P., Andrews, O. D., Arora, V. K., Bakker, D. C. E., Barbero, L., Becker, M., Betts, R. A., Bopp, L., Chevallier, F., Chini, L. P., Ciais, P., Cosca, C. E., Cross, J., Currie, K., Gasser, T., Harris, I., Hauck, J., Haverd, V., Houghton, R. A., Hunt, C. W., Hurtt, G., Ilyina, T., Jain, A. K., Kato, E., Kautz, M., Keeling, R. F., Klein Goldewijk, K., Körtzinger, A., Landschützer, P., Lefèvre, N., Lenton, A., Lienert, S., Lima, I., Lombardozzi, D., Metzl, N., Millero, F., Monteiro, P. M. S., Munro, D. R., Nabel, J. E. M. S., Nakaoka, S., Nojiri, Y., Padin, X. A., Peregon, A., Pfeil, B., Pierrot, D., Poulter, B., Rehder, G., Reimer, J., Rödenbeck, C., Schwinger, J., Séférian, R., Skjelvan, I., Stocker, B. D., Tian, H., Tilbrook, B., Tubiello, F. N., van der Laan-Luijkx, I. T., van der Werf, G. R., van Heuven, S., Viovy, N., Vuichard, N., Walker, A. P., Watson, A. J., Wiltshire, A. J., Zachle, S., and Zhu, D.: Global Carbon Budget 2017, *Earth Syst. Sci. Data*, 10, 405–448, <https://doi.org/10.5194/essd-10-405-2018>, 2018.
- Li, Q., Tietema, A., Reinsch, S., Schmidt, I. K., de Dato, G., Guidolotti, G., Lellei-Kovács, E., Kopittke, G., and Larsen, K. S.: Higher sensitivity of gross primary productivity than ecosystem respiration to experimental drought and warming across six European shrubland ecosystems, *Sci. Total Environ.*, 900, 165627, <https://doi.org/10.1016/j.scitotenv.2023.165627>, 2023.
- Lienert, S. and Joos, F.: A Bayesian ensemble data assimilation to constrain model parameters and land-use carbon emissions, *Biogeosciences*, 15, 2909–2930, <https://doi.org/10.5194/BG-15-2909-2018>, 2018.
- Lin, S., Hu, Z., Wang, Y., Chen, X., He, B., Song, Z., Sun, S., Wu, C., Zheng, Y., Xia, X., Liu, L., Tang, J., Sun, Q., Joos, F., and Yuan, W.: Underestimated Interannual Variability of Terrestrial Vegetation Production by Terrestrial Ecosystem Models, *Global Biogeochem. Cycles*, 37, e2023GB007696, <https://doi.org/10.1029/2023GB007696>, 2023.
- Lindeskog, M., Smith, B., Lagergren, F., Sycheva, E., Ficko, A., Pretzsch, H., and Rammig, A.: Accounting for forest management in the estimation of forest carbon balance using the dynamic vegetation model LPJ-GUESS (v4.0, r9710): Implementation and evaluation of simulations for Europe, 6071–6112 pp., <https://doi.org/10.5194/gmd-14-6071-2021>, 2021.
- Longo, M., Knox, R. G., Medvigy, D. M., Levine, N. M., Dietze, M. C., Kim, Y., Swann, A. L. S., Zhang, K., Rollinson, C. R., Bras, R. L., Wofsy, S. C., and Moorcroft, P. R.: The biophysics, ecology, and biogeochemistry of functionally diverse, vertically and horizontally heterogeneous ecosystems: The Ecosystem Demography model, version 2.2-Part 1: Model description, *Geosci. Model Dev.*, 12, 4309–4346, <https://doi.org/10.5194/GMD-12-4309-2019>, 2019.
- Madani, N., Kimball, J. S., Jones, L. A., Parazoo, N. C., and Guan, K.: Global Analysis of Bioclimatic Controls on Ecosystem Productivity Using Satellite Observations of Solar-Induced Chlorophyll Fluorescence, *Remote Sens.* 2017, Vol. 9, Page 530, 9, 530, <https://doi.org/10.3390/RS9060530>, 2017.
- Martinez del Castillo, E., Zang, C. S., Buras, A., Hacket-Pain, A., Esper, J., Serrano-Notivoli, R., Hartl, C., Weigel, R., Klesse, S., Resco de Dios, V., Scharnweber, T., Dorado-Liñán, I., van der Maaten-Theunissen, M., van der Maaten, E., Jump, A., Mikac, S., Banzragch, B. E., Beck, W., Cavin, L., Claessens, H., Čada, V., Čufar, K., Dulamsuren, C., Gričar, J., Gil-Pelegrín, E., Janda, P., Kazimirovic, M., Kreyling, J., Latte, N., Leuschner, C., Longares, L. A., Menzel, A., Merela, M., Motta, R., Muffler, L., Nola, P., Petritan, A. M., Petritan, I. C., Prislan, P., Rubio-Cuadrado, Á., Rydval, M., Stajić, B., Svoboda, M., Toromani, E., Trotsiuk, V., Wilmking, M., Zlatanov, T., and de Luis, M.: Climate-change-driven growth decline of European beech forests, *Commun. Biol.* 2022 51, 5, 1–9, <https://doi.org/10.1038/s42003-022-03107-3>, 2022.
- Messori, G., Ruiz-Pérez, G., Manzoni, S., and Vico, G.: Climate drivers of the terrestrial carbon cycle variability

1201 in Europe, *Environ. Res. Lett.*, 14, 063001, <https://doi.org/10.1088/1748-9326/AB1AC0>, 2019.

1202

1203 Monteith, J. and Unsworth, M.: *Principles of Environmental Physics* - 3rd Edition, Academic Press, 440 pp., 2007.

1204

1205 Muñoz Sabater, J.: ERA5-Land hourly data from 1950 to present. Copernicus Climate Change Service (C3S)

1206 Climate Data Store (CDS), <https://doi.org/10.24381/cds.e2161bac>, 2019.

1207

1208 Nelson, J. A., Walther, S., Gans, F., Kraft, B., Weber, U., Novick, K., Buchmann, N., Migliavacca, M., Wohlfahrt,

1209 G., Šigut, L., Ibrom, A., Papale, D., Göckede, M., Duveiller, G., Knohl, A., Hörtnagl, L., Scott, R. L., Dušek,

1210 J., Zhang, W., Hamdi, Z. M., Reichstein, M., Aranda-Barranco, S., Ardö, J., Op de Beeck, M., Billesbach, D.,

1211 Bowling, D., Bracho, R., Brümmer, C., Camps-Valls, G., Chen, S., Cleverly, J. R., Desai, A., Dong, G., El-

1212 Madany, T. S., Euskirchen, E. S., Feigenwinter, I., Galvagno, M., Gerosa, G. A., Gielen, B., Goded, I., Goslee,

1213 S., Gough, C. M., Heinesch, B., Ichii, K., Jackowicz-Korczynski, M. A., Klosterhalfen, A., Knox, S.,

1214 Kobayashi, H., Kohonen, K.-M., Korkiakoski, M., Mammarella, I., Gharun, M., Marzuoli, R., Matamala, R.,

1215 Metzger, S., Montagnani, L., Nicolini, G., O'Halloran, T., Ourcival, J.-M., Peichl, M., Pendall, E., Ruiz

1216 Reverter, B., Roland, M., Sabbatini, S., Sachs, T., Schmidt, M., Schwalm, C. R., Shekhar, A., Silberstein, R.,

1217 Silveira, M. L., Spano, D., Tagesson, T., Tramontana, G., Trotta, C., Turco, F., Vesala, T., Vincke, C., Vitale,

1218 D., Vivoni, E. R., Wang, Y., Woodgate, W., Yezpe, E. A., Zhang, J., Zona, D., and Jung, M.: X-BASE: the

1219 first terrestrial carbon and water flux products from an extended data-driven scaling framework, *FLUXCOM-*

1220 *X*, *Biogeosciences*, 21, 5079–5115, <https://doi.org/10.5194/BG-21-5079-2024>, 2024.

1221

1222 Pan, Y., Birdsey, R. A., Phillips, O. L., Houghton, R. A., Fang, J., Kauppi, P. E., Keith, H., Kurz, W. A., Ito, A.,

1223 Lewis, S. L., Nabuurs, G.-J., Shvidenko, A., Hashimoto, S., Lerink, B., Schepaschenko, D., Castanho, A., and

1224 Murdiyarso, D.: The enduring world forest carbon sink, *Nature*, 631, 563–569,

1225 <https://doi.org/10.1038/s41586-024-07602-x>, 2024.

1226

1227 Pastorello, G., Trotta, C., Canfora, E., Chu, H., Christianson, D., Cheah, Y. W., Poindexter, C., Chen, J.,

1228 Elbashandy, A., Humphrey, M., Isaac, P., Polidori, D., Ribeca, A., van Ingen, C., Zhang, L., Amiro, B.,

1229 Ammann, C., Arain, M. A., Ardö, J., Arkebauer, T., Arndt, S. K., Arriga, N., Aubinet, M., Aurela, M.,

1230 Baldocchi, D., Barr, A., Beamesderfer, E., Marchesini, L. B., Bergeron, O., Beringer, J., Bernhofer, C.,

1231 Berveiller, D., Billesbach, D., Black, T. A., Blanken, P. D., Bohrer, G., Boike, J., Bolstad, P. V., Bonal, D.,

1232 Bonnefond, J. M., Bowling, D. R., Bracho, R., Brodeur, J., Brümmer, C., Buchmann, N., Burban, B., Burns,

1233 S. P., Buysse, P., Cale, P., Cavagna, M., Cellier, P., Chen, S., Chini, I., Christensen, T. R., Cleverly, J., Collalti,

1234 A., Consalvo, C., Cook, B. D., Cook, D., Coursolle, C., Cremonese, E., Curtis, P. S., D'Andrea, E., da Rocha,

1235 H., Dai, X., Davis, K. J., De Cinti, B., de Grandcourt, A., De Ligne, A., De Oliveira, R. C., Delpierre, N.,

1236 Desai, A. R., Di Bella, C. M., di Tommasi, P., Dolman, H., Domingo, F., Dong, G., Dore, S., Duce, P.,

1237 Dufrêne, E., Dunn, A., Dušek, J., Eamus, D., Eichmann, U., ElKhidir, H. A. M., Eugster, W., Ewenz, C. M.,

1238 Ewers, B., Famulari, D., Fares, S., Feigenwinter, I., Feitz, A., Fensholt, R., Filippa, G., Fischer, M., Frank, J.,

1239 Galvagno, M., Gharun, M., Gianelle, D., et al.: The FLUXNET2015 dataset and the ONEFlux processing

1240 pipeline for eddy covariance data, *Sci. Data* 2020 71, 7, 1–27, <https://doi.org/10.1038/s41597-020-0534-3>,

1241 2020.

1242

1243 Piao, S., Ciais, P., Friedlingstein, P., De Noblet-Ducoudré, N., Cadule, P., Viovy, N., and Wang, T.:

1244 Spatiotemporal patterns of terrestrial carbon cycle during the 20th century, *Global Biogeochem. Cycles*, 23,

1245 <https://doi.org/10.1029/2008GB003339>, 2009.

1246

1247 Prentice, I. C., Farquhar, G. D., Fasham, M. J. R., Goulden, M. L., Heimann, M., Jaramillo, V. J., Kheshgi, H. S.,

1248 Le Quéré, C., Scholes, R. J., Contributing, D. W. R. W., Archer, D., Ashmore, M. R., Aumont, O., Baker, D.,

1249 Battle, M., Bender, M., Bopp, L. P., Bousquet, P., Caldeira, K., Ciais, P., Cox, P. M., Cramer, W., Dentener,

1250 F., Enting, I. G., Field, C. B., Friedlingstein, P., Holland, E. A., Houghton, R. A., House, J. I., Ishida, A., Jain,

1251 A. K., Janssens, I. A., Joos, F., Kaminski, T., Keeling, C. D., Keeling, R. F., Kicklighter, D. W., Kohfeld, K.

1252 E., Knorr, W., Law, R., Lenton, T., Lindsay, K., Maier-Reimer, E., Manning, A. C., Matear, R. J., McGuire,

1253 A. D., Melillo, J. M., Meyer, R., Mund, M., Orr, J. C., Piper, S., Plattner, K., Rayner, P. J., Sitch, S., Slater,

1254 R., Taguchi, S., Tans, P. P., Tian, H. Q., Weirig, M. F., Whorf, T., Review, A. Y., Pitelka, E. L., and Rojas,

1255 A. R.: The Carbon Cycle and Atmospheric Carbon Dioxide, in *Climate Change 2001: The Scientific Basis.*

1256 *Contribution of Working Group I to the Third Assessment Report of the Intergovernmental Panel on Climate*

1257 *Change*, 183–237 pp., 2001.

1258

1259 Pugh, T. A. M., Lindeskog, M., Smith, B., Poulter, B., Arneth, A., Haverd, V., and Calle, L.: Role of forest

Code de champ modifié

regrowth in global carbon sink dynamics, *Proc. Natl. Acad. Sci. U. S. A.*, 116, 4382–4387, [https://doi.org/10.1073/PNAS.1810512116/SUPPL\\_FILE/PNAS.1810512116.SD02.TXT](https://doi.org/10.1073/PNAS.1810512116/SUPPL_FILE/PNAS.1810512116.SD02.TXT), 2019.

Saunders, M., Tobin, B., Black, K., Gioria, M., Nieuwenhuis, M., and Osborne, B. A.: Thinning effects on the net ecosystem carbon exchange of a Sitka spruce forest are temperature-dependent, *Agric. For. Meteorol.*, 157, 1–10, <https://doi.org/10.1016/J.AGRFORMET.2012.01.008>, 2012.

Schimel, D., Stephens, B. B., and Fisher, J. B.: Effect of increasing CO<sub>2</sub> on the terrestrial carbon cycle, *Proc. Natl. Acad. Sci. U. S. A.*, 112, 436–441, [https://doi.org/10.1073/PNAS.1407302112/SUPPL\\_FILE/PNAS.201407302SI.PDF](https://doi.org/10.1073/PNAS.1407302112/SUPPL_FILE/PNAS.201407302SI.PDF), 2015.

Seddon, A. W. R., Macias-Fauria, M., Long, P. R., Benz, D., and Willis, K. J.: Sensitivity of global terrestrial ecosystems to climate variability, *Nat.* 2016 5317593, 531, 229–232, <https://doi.org/10.1038/nature16986>, 2016.

Seiler, C., Melton, J. R., Arora, V. K., and Wang, L.: CLASSIC v1.0: The open-source community successor to the Canadian Land Surface Scheme (CLASS) and the Canadian Terrestrial Ecosystem Model (CTEM) - Part 2: Global benchmarking, *Geosci. Model Dev.*, 14, 2371–2417, <https://doi.org/10.5194/GMD-14-2371-2021>, 2021.

Sharma, B., Kumar, J., Collier, N., Ganguly, A. R., and Hoffman, F. M.: Quantifying Carbon Cycle Extremes and Attributing Their Causes Under Climate and Land Use and Land Cover Change From 1850 to 2300, *J. Geophys. Res. Biogeosciences*, 127, e2021JG006738, <https://doi.org/10.1029/2021JG006738>, 2022.

Sitch, S., Huntingford, C., Gedney, N., Levy, P. E., Lomas, M., Piao, S. L., Betts, R., Ciais, P., Cox, P., Friedlingstein, P., Jones, C. D., Prentice, I. C., and Woodward, F. I.: Evaluation of the terrestrial carbon cycle, future plant geography and climate-carbon cycle feedbacks using five Dynamic Global Vegetation Models (DGVMs), *Glob. Chang. Biol.*, 14, 2015–2039, <https://doi.org/10.1111/J.1365-2486.2008.01626.X>, 2008.

Sitch, S., O’Sullivan, M., Robertson, E., Friedlingstein, P., Albergel, C., Anthoni, P., Arneeth, A., Arora, V. K., Bastos, A., Bastrikov, V., Bellouin, N., Canadell, J. G., Chini, L., Ciais, P., Falk, S., Harris, I., Hurtt, G., Ito, A., Jain, A. K., Jones, M. W., Joos, F., Kato, E., Kennedy, D., Klein Goldewijk, K., Kluzek, E., Knauer, J., Lawrence, P. J., Lombardozzi, D., Melton, J. R., Nabel, J. E. M. S., Pan, N., Peylin, P., Pongratz, J., Poulter, B., Rosan, T. M., Sun, Q., Tian, H., Walker, A. P., Weber, U., Yuan, W., Yue, X., and Zaehle, S.: Trends and Drivers of Terrestrial Sources and Sinks of Carbon Dioxide: An Overview of the TRENDY Project, *Global Biogeochem. Cycles*, 38, e2024GB008102, <https://doi.org/10.1029/2024GB008102>, 2024.

Smith, N. E., Kooijmans, L. M. J., Koren, G., Van Schaik, E., Van Der Woude, A. M., Wanders, N., Ramonet, M., Xueref-Remy, I., Siebicke, L., Manca, G., Brümmer, C., Baker, I. T., Haynes, K. D., Luijkx, I. T., and Peters, W.: Spring enhancement and summer reduction in carbon uptake during the 2018 drought in northwestern Europe, *Philos. Trans. R. Soc. B*, 375, <https://doi.org/10.1098/RSTB.2019.0509>, 2020.

Tang, X., Li, H., Desai, A. R., Nagy, Z., Luo, J., Kolb, T. E., Oliso, A., Xu, X., Yao, L., Kutsch, W., Pilegaard, K., Köstner, B., and Ammann, C.: How is water-use efficiency of terrestrial ecosystems distributed and changing on Earth?, *Sci. Reports* 2014 41, 4, 1–11, <https://doi.org/10.1038/srep07483>, 2014.

Team, W. W., and Centre, I. E. T.: Warm Winter 2020 ecosystem eddy covariance flux product for 73 stations in FLUXNET-Archive format—release 2022-1, <https://doi.org/https://doi.org/10.18160/2G60-ZHAK>, 2022.

Thompson, R. L., Broquet, G., Gerbig, C., Koch, T., Lang, M., Monteil, G., Munassar, S., Nickless, A., Scholze, M., Ramonet, M., Karstens, U., Van Schaik, E., Wu, Z., and Rödenbeck, C.: Changes in net ecosystem exchange over Europe during the 2018 drought based on atmospheric observations, *Philos. Trans. R. Soc. B*, 375, <https://doi.org/10.1098/RSTB.2019.0512>, 2020.

Tian, H., Lu, C., Ciais, P., Michalak, A. M., Canadell, J. G., Saikawa, E., Huntzinger, D. N., Gurney, K. R., Sitch, S., Zhang, B., Yang, J., Bousquet, P., Bruhwiler, L., Chen, G., Dlugokencky, E., Friedlingstein, P., Melillo, J., Pan, S., Poulter, B., Prinn, R., Saunio, M., Schwalm, C. R., and Wofsy, S. C.: The terrestrial biosphere as a net source of greenhouse gases to the atmosphere, *Nat.* 2016 5317593, 531, 225–228, <https://doi.org/10.1038/nature16946>, 2016.

Tramontana, G., Jung, M., Schwalm, C. R., Ichii, K., Camps-Valls, G., Ráduly, B., Reichstein, M., Arain, M. A., Cescatti, A., Kiely, G., Merbold, L., Serrano-Ortiz, P., Sickert, S., Wolf, S., and Papale, D.: Predicting carbon dioxide and energy fluxes across global FLUXNET sites with regression algorithms, *Biogeosciences*, 13, 4291–4313, <https://doi.org/10.5194/BG-13-4291-2016>, 2016.

van der Woude, A. M., Peters, W., Joetjzer, E., Lafont, S., Koren, G., Ciais, P., Ramonet, M., Xu, Y., Bastos, A., Botia, S., Sitch, S., de Kok, R., Kneuer, T., Kubistin, D., Jacotot, A., Loubet, B., Herig-Coimbra, P. H., Loustau, D., and Luijkx, I. T.: Temperature extremes of 2022 reduced carbon uptake by forests in Europe, *Nat. Commun.* 2023 141, 14, 1–11, <https://doi.org/10.1038/s41467-023-41851-0>, 2023.

von Buttlar, J., Zscheischler, J., Rammig, A., Sippel, S., Reichstein, M., Knohl, A., Jung, M., Menzer, O., Arain, M. A., Buchmann, N., Cescatti, A., Gianelle, D., Kiely, G., Law, B. E., Magliulo, V., Margolis, H., McCaughey, H., Merbold, L., Migliavacca, M., Montagnani, L., Oechel, W., Pavelka, M., Peichl, M., Rambal, S., Raschi, A., Scott, R. L., Vaccari, F. P., Van Gorsel, E., Varlagin, A., Wohlfahrt, G., and Mahecha, M. D.: Impacts of droughts and extreme-temperature events on gross primary production and ecosystem respiration: a systematic assessment across ecosystems and climate zones, *Biogeosciences*, 15, 1293–1318, <https://doi.org/10.5194/bg-15-1293-2018>, 2018.

Walker, A. P., De Kauwe, M. G., Bastos, A., Belmecheri, S., Georgiou, K., Keeling, R. F., McMahon, S. M., Medlyn, B. E., Moore, D. J. P., Norby, R. J., Zachle, S., Anderson-Teixeira, K. J., Battipaglia, G., Brien, R. J. W., Cabugao, K. G., Cailleret, M., Campbell, E., Canadell, J. G., Ciais, P., Craig, M. E., Ellsworth, D. S., Farquhar, G. D., Faticchi, S., Fisher, J. B., Frank, D. C., Graven, H., Gu, L., Haverd, V., Heilman, K., Heimann, M., Hungate, B. A., Iversen, C. M., Joos, F., Jiang, M., Keenan, T. F., Knauer, J., Körner, C., Leshyk, V. O., Leuzinger, S., Liu, Y., MacBean, N., Malhi, Y., McVicar, T. R., Penuelas, J., Pongratz, J., Powell, A. S., Riutta, T., Sabot, M. E. B., Schleucher, J., Sitch, S., Smith, W. K., Sulman, B., Taylor, B., Terrer, C., Torn, M. S., Treseder, K. K., Trugman, A. T., Trumbore, S. E., van Mantgem, P. J., Voelker, S. L., Whelan, M. E., and Zuidema, P. A.: Integrating the evidence for a terrestrial carbon sink caused by increasing atmospheric CO<sub>2</sub>, *New Phytol.*, 229, 2413–2445, <https://doi.org/10.1111/NPH.16866>, 2021.

Wang, J., Chen, J., Zhang, J., Yang, S., Zhang, S., Bai, Y., and Xu, R.: Consistency and uncertainty of remote sensing-based approaches for regional yield gap estimation: A comprehensive assessment of process-based and data-driven models, *F. Crop. Res.*, 302, 109088, <https://doi.org/10.1016/J.FCR.2023.109088>, 2023.

Welp, L. R., Randerson, J. T., and Liu, H. P.: The sensitivity of carbon fluxes to spring warming and summer drought depends on plant functional type in boreal forest ecosystems, *Agric. For. Meteorol.*, 147, 172–185, <https://doi.org/10.1016/J.AGRFORMET.2007.07.010>, 2007.

Woodward, F. I. and Lomas, M. R.: Vegetation dynamics--simulating responses to climatic change, *Biol. Rev. Camb. Philos. Soc.*, 79, 643–670, <https://doi.org/10.1017/S1464793103006419>, 2004.

Wu, Z., Ahlström, A., Smith, B., Ardö, J., Eklundh, L., Fensholt, R., and Lehsten, V.: Climate data induced uncertainty in model-based estimations of terrestrial primary productivity, *Environ. Res. Lett.*, 12, 064013, <https://doi.org/10.1088/1748-9326/AA6FD8>, 2017.

Xia, J., Chen, Y., Liang, S., Liu, D., and Yuan, W.: Global simulations of carbon allocation coefficients for deciduous vegetation types, *Tellus B Chem. Phys. Meteorol.*, 6, <https://doi.org/10.3402/TELLUSB.V67.28016>, 2015.

Xu, S., Gentile, P., Li, L., Wang, L., Yu, Z., Dong, N., Ju, Q., and Zhang, Y.: Response of Ecosystem Productivity to High Vapor Pressure Deficit and Low Soil Moisture: Lessons Learned From the Global Eddy-Covariance Observations, *Earth's Futur.*, 11, e2022EF003252, <https://doi.org/10.1029/2022EF003252>, 2023.

Zachle, S., Friend, A. D., Friedlingstein, P., Dentener, F., Peylin, P., and Schulz, M.: Carbon and nitrogen cycle dynamics in the O-CN land surface model: 2. Role of the nitrogen cycle in the historical terrestrial carbon balance, *Global Biogeochem. Cycles*, 24, 1006, <https://doi.org/10.1029/2009GB003522>, 2010.

Zhuravlev, R., Dara, A., Santos, A. L. D. dos, Demidov, O., and Burba, G.: Globally Scalable Approach to Estimate Net Ecosystem Exchange Based on Remote Sensing, Meteorological Data, and Direct Measurements of Eddy Covariance Sites, *Remote Sens.* 2022, Vol. 14, Page 5529, 14, 5529, <https://doi.org/10.3390/RS14215529>, 2022.

**a supprimé:** Valentini, R., Arneth, A., Bombelli, A., Castaldi, S., Cazzolla Gatti, R., Chevallier, F., Ciais, P., Grieco, E., Hartmann, J., Henry, M., Houghton, R. A., Jung, M., Kutsch, W. L., Malhi, Y., Mayorga, E., Merbold, L., Murray-Tortarolo, G., Papale, D., Peylin, P., Poulter, B., Raymond, P. A., Santini, M., Sitch, S., Vaglio Laurin, G., Van Der Werf, G. R., Williams, C. A., and Scholes, R. J.: A full greenhouse gases budget of africa: Synthesis, uncertainties, and vulnerabilities, *Biogeosciences*, 11, 381–407, <https://doi.org/10.5194/BG-11-381-2014>, 2014.

Code de champ modifié

1391  
1392